Competing Atmospheric and Surface-Driven Impacts of Absorbing Aerosols on the East Asian Summertime Climate

GEETA G. PERSAD

Carnegie Institution for Science, Stanford, California

DAVID J. PAYNTER, YI MING, AND V. RAMASWAMY

NOAA/Geophysical Fluid Dynamics Laboratory, Princeton, New Jersey

(Manuscript received 1 December 2016, in final form 1 August 2017)

ABSTRACT

East Asia has some of the largest concentrations of absorbing aerosols globally, and these, along with the region's scattering aerosols, have both reduced the amount of solar radiation reaching Earth's surface regionally (solar dimming) and increased shortwave absorption within the atmosphere, particularly during the peak months of the East Asian summer monsoon (EASM). This study analyzes how atmospheric absorption and surface solar dimming compete in driving the response of regional summertime climate to anthropogenic aerosols, which dominates, and why—issues of particular importance for predicting how East Asian climate will respond to projected changes in absorbing and scattering aerosol emissions in the future. These questions are probed in a state-of-the-art general circulation model using a combination of realistic and novel idealized aerosol perturbations that allow analysis of the relative influence of absorbing aerosols' atmospheric and surface-driven impacts on regional circulation and climate. Results show that even purely absorption-driven dimming decreases EASM precipitation by cooling the land surface, counteracting climatological land–sea contrast and reducing ascending atmospheric motion and onshore winds, despite the associated positive top-of-the-atmosphere regional radiative forcing. Absorption-driven atmospheric heating does partially offset the precipitation and surface evaporation reduction from surface dimming, but the overall response to aerosol absorption more closely resembles the response to its surface dimming than to its atmospheric heating. These findings provide a novel decomposition of absorbing aerosol's impacts on regional climate and demonstrate that the response cannot be expected to follow the sign of absorption's top-of-the-atmosphere or even atmospheric radiative perturbation.

1. Introduction

East Asia receives approximately half of its annual precipitation during the summer months of June, July, and August. The summertime maximum in solar radiation warms the East Asian continent more rapidly than the adjacent ocean as a result of the land's lower heat capacity, setting up temperature and pressure gradients that drive onshore flow of moisture and ascending atmospheric motion over the continent (e.g., Webster 1987). This land–sea thermal contrast, combined with orographic forcing and seasonal shifts in the subtropical westerly jet and western Pacific subtropical high, produces a precipitation maximum that peaks in June and July over East Asia, known collectively as the East Asian summer monsoon (EASM) (e.g., Tao and Chen 1987; Chen and Bordoni 2014).

Superimposed on this climatological picture are changes in the radiative environment resulting from anthropogenic emissions over the last several decades. Atmospheric concentrations of absorbing and scattering anthropogenic aerosols in East Asia are second only to those in South Asia (e.g., Streets et al. 2009). Aerosol concentrations over the East Asian subcontinent decreased the annual mean clear-sky surface solar radiation (e.g., Qian et al. 2006, 2007) by 4.3 $W m^{-2}$ $decade^{-1}$ from the 1960s to the 2000s according to recent estimates (Allen et al. 2013). This ''solar dimming'' counteracts the climatological land–sea thermal contrast by cooling the land surface more rapidly than the adjacent ocean, both resulting from the land's lower heat capacity and because the aerosol is more strongly concentrated over land than over ocean (e.g., Guo et al. 2013; Wang

Corresponding author: Geeta G. Persad, gpersad@carnegiescience.edu

DOI: 10.1175/JCLI-D-16-0860.1

et al. 2015). Several modeling studies have suggested that anthropogenic aerosol emissions over East Asia could be the primary contributor to a weakening in EASM circulation and precipitation since the middle of the twentieth century (e.g., Song et al. 2014; Wang et al. 2015), although this effect remains uncertain (Kim et al. 2016; Ma et al. 2017) and other factors—such as global sea surface temperature changes—are thought to play a substantial role (e.g., Li et al. 2010).

Recent work, however, has demonstrated that as much as half of the observed clear-sky reduction in surface solar radiation is due to the absorption of solar radiation within the atmospheric column by absorbing aerosols, as opposed to the reflection of that radiation back to space through scattering. Persad et al. (2014) identify in general circulation model (GCM) simulations that aerosol absorption under clear-sky conditions increased over East Asia by approximately 1.6 $W m^{-2}$ $decade^{-1}$ from the 1960s to the 2000s, robust across different model aerosol formulations. Consequently, during the 2000s, the presence of anthropogenic aerosols (both scattering and absorbing) decreased East Asian summertime clear-sky surface solar radiation by approximately 20 $W m^{-2}$ and increased atmospheric absorption by approximately 10 $W m^{-2}$. This vertical radiative dipole of atmospheric heating and surface dimming might be expected to have a substantially different impact on regional summertime circulation and precipitation than surface dimming or atmospheric heating on its own, but the effects of this dipole have not been cleanly decomposed before now.

The ''semidirect effect'' of absorbing aerosols, whereby the atmospheric radiative heating from direct aerosol absorption changes the thermodynamic and dynamical environment for cloud formation, is well known (e.g., Hansen et al. 1997; Koch and Del Genio 2010). Studies show that this atmospheric heating can either invigorate or suppress convection, depending on the altitude of the heating relative to the climatological cloud (e.g., Johnson et al. 2004; Feingold 2005; Persad et al. 2012). Depending on the convective environment, atmospheric heating on its own has been shown to induce strong rising atmospheric motion regionally that promotes monsoonal moisture flux and convective precipitation (Chung et al. 2002; Wang 2004; Erlick et al. 2006; Meehl et al. 2008).

However, the same absorption process via which these aerosols heat the atmosphere also reduces the shortwave radiation at the surface, and it is unclear how these two effects will interact regionally. On its own, solar dimming reduces both land-surface temperature and the surface energy available for latent and sensible heat fluxes that help drive convection and precipitation (e.g., Roeckner et al. 1999; Huang et al. 2007). In a global mean sense, solar dimming from purely scattering aerosols has been shown to spin down the hydrological cycle (Ramanathan et al. 2001). Depending on the degree of coupling between the surface and atmosphere, atmospheric heating from absorption may or may not be communicated to the surface and counteract the surface temperature effects of the solar dimming (Ramanathan and Carmichael 2008). In the case of weak coupling, the combination of surface cooling and atmospheric heating from aerosol absorption can reduce surface-air temperature and humidity gradients that drive evaporation, thus limiting the moisture available for rainfall (Ramanathan et al. 2005).

Given these uncertainties and the large absorbing aerosol concentrations in East Asia, a robust understanding of the separate, combined, and competing effects of atmospheric heating and surface dimming from aerosol absorption on the East Asian summertime climate is of crucial importance but until now has been limited. The relative effect of absorbing black carbon and scattering sulfate aerosols on East Asian climate has been studied previously in a range of climate models (e.g., Huang et al. 2007; Randles and Ramaswamy 2008; Guo et al. 2013; Jiang et al. 2013; Wang et al. 2015). However, the total shortwave absorption resulting from black carbon in models and the resulting ratio of surface dimming to atmospheric heating remains uncertain (Bond et al. 2013). Separate analysis of surface dimming and of atmospheric heating in monsoonal systems has shown substantially different impacts on regional climate (e.g., Chung et al. 2002; Roeckner et al. 1999). However, the coupled effects of the two may be quite different than the sum of the parts. A holistic analysis of the separate and combined impacts of surface dimming and atmospheric heating is thus a crucial and missing element of a more robust understanding of absorbing aerosol impacts on the EASM and East Asian summertime climate in general.

We here isolate and analyze the surface- versus atmosphere-driven impacts of aerosol absorption on East Asian summertime climate, using a combination of realistic and idealized forcing simulations in a state-of-the-art climate model, to address the following questions. What are the competing effects on the EASM of increased atmospheric absorption and decreased surface solar radiation resulting from recent regional aerosol emissions? Does the atmospheric heating from aerosol absorption enhance or counteract the circulation effects of aerosol-driven solar dimming on the EASM? Which wins, and why? These are questions of interest both to present-day understanding of the forcers of East Asian climate variability and to our predictive ability to

understand how future changes in aerosol characteristics over East Asia will affect its projected regional climate.

2. Methods

We conduct simulations using both realistic historical aerosol emissions and idealized perturbations in the Geophysical Fluid Dynamics Laboratory's (GFDL) atmospheric general circulation model [Atmospheric Model, version 3 (AM3); Donner et al. 2011]. In brief, we use a historical aerosol-only simulation to derive the signal of surface dimming, atmospheric heating, and atmospheric absorption over East Asia as a result of regional aerosol emissions. Aerosol-induced surface dimming in this model has been validated against observations in Allen et al. (2013) and Persad et al. (2014), and overall aerosol properties have been compared with observations in Donner et al. (2011). We then use the simulated regional aerosol signal to construct a set of idealized forcing simulations in which we separately impose either surface dimming, atmospheric heating, or atmospheric absorption (inducing both dimming and heating) over East Asia.

Full details of the GFDL AM3 model may be found in Donner et al. (2011), but we here summarize aspects central to this study. GFDL AM3's horizontal grid is a cubed sphere, with grid size varying from 163 to 231 km, and its atmosphere contains 48 vertical layers. Crucially for this analysis, GFDL AM3 has been found to outperform other models in its CMIP generation in simulating twentieth-century clear-sky solar dimming over East Asia (Allen et al. 2013) via a substantial contribution from aerosol absorption (Persad et al. 2014), making it a reasonable tool with which to investigate the competing effects of aerosol dimming and absorption on the EASM. The GFDL CM3 model suite has been previously used to study East Asian summer climate as part of the CMIP5 model suite (Sperber et al. 2013; Salzmann et al. 2014; Li et al. 2015). The CMIP5-generation models exhibit greater skill than previous generations in capturing monsoon rainfall and circulation climatology, achieving approximately 90% agreement with observed precipitation, although biases remain in representation of the monsoonal trough, mei-yu front, and meridional precipitation structure (Sperber et al. 2013; Song and Zhou 2014). GFDL CM3 is among the top-five CMIP5 models in terms of skill in simulating climatological Asian summer monsoon precipitation characteristics over the region and time period analyzed in this study (Sperber et al. 2013). Additionally, over East Asia, GFDL AM3 exhibits relatively small biases in comparison with observations in monsoon-critical parameters such as 500-mb geopotential height, surface air temperature, and precipitation (Donner et al. 2011).

Aerosol emissions are fully interactive in GFDL AM3; that is, prescribed aerosol emissions are transported, aged, and removed according to the internal meteorology and chemistry of the model. To compute radiative properties, black carbon (BC) and sulfate aerosol are assumed to be internally mixed using a uniform mixing scheme, which calculates the refractive index of the mixed aerosol as the volume-weighted average of BC and sulfate. All other aerosols are treated as externally mixed. BC is the strongest absorber in GFDL AM3 (Ocko et al. 2012), although organic carbon is also slightly absorbing in the model's formulation (Donner et al. 2011). The model contains aerosol indirect effects with sulfate, sea salt, and organic carbon aerosols acting as cloud condensation nuclei according to the parameterization of Ming et al. (2006) and Ming et al. (2007).

We first derive realistic regional aerosol effects from an ensemble of historical single forcing simulations with time-varying sea surface temperature (SST) and sea ice prescribed from the Hadley Centre Sea Ice and Sea Surface Temperature, version 1 (HadISST1), observational dataset (Rayner et al. 2003). The simulations are 1) a five-member control ensemble with all anthropogenic emissions fixed at preindustrial (1860) values (FIXED) and 2) a five-member ensemble of experiments with historically varying anthropogenic aerosol emissions from Lamarque et al. (2010) over China (AERO_C; as defined by national boundaries, roughly 20°–50°N, 75°–125°E) but all other anthropogenic emissions (i.e., well-mixed greenhouse gases and ozone, plus all aerosol emissions outside of China) fixed at preindustrial (1860) values as in FIXED. The FIXED ensemble is run from 1860–2005. The AERO_C ensemble is branched from a FIXED simulation at 1970 and run through 2000. The realistic regional aerosol signal, hereafter referred to as "realistic aerosol," is calculated as the 1981–2000 average ensemble-mean values from the AERO_C ensemble minus the FIXED ensemble.

The realistic regional aerosols produce average column burdens of about $10\,mg\,m^{-2}$ of scattering sulfate and about $1\,mg\,m^{-2}$ of absorbing black carbon aerosol over East Asia, which absorb and scatter incoming shortwave radiation, resulting in both absorption- and scattering-driven surface dimming and absorption-driven atmospheric heating (section 4). We next use the aerosol radiative effects from the realistic aerosol signal to construct a series of idealized forcing simulations that allow us to isolate the effects of these different components of aerosols' radiative perturbation on East Asian summertime climate. The control simulation for

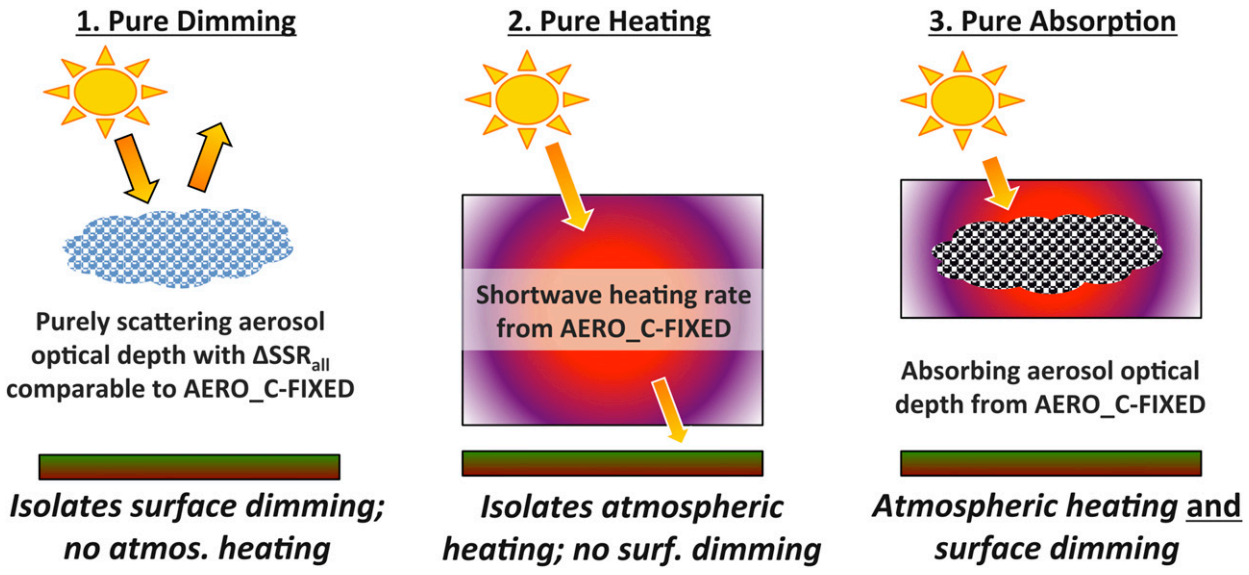

FIG. 1. The three idealized forcing perturbations are schematically depicted. Each of the depicted perturbations is imposed over southeastern China (22.5°–40°N, 100°–122.5°E) during years 1980–2000 of an ALL control simulation, which contains historically varying anthropogenic and natural emissions and observationally prescribed sea surface temperature and sea ice.

these is a historical simulation (ALL) run from 1860–2005 with time-varying sea surface temperature and sea ice as in FIXED but with all natural and anthropogenic forcers varying historically [see Donner et al. (2011) for inventories from which emissions are derived]. Onto this ALL control simulation, each of the three idealized perturbations described below is imposed in the years 1980–2000 over southeastern China (22.5°–40°N, 100°–122.5°E)—the region of maximum aerosol emissions and radiative forcing in East Asia (Streets et al. 2013), as well as maximum climatological EASM precipitation. This is also the region of greatest observational coverage (Allen et al. 2013; Norris and Wild 2009; Dwyer et al. 2010) and one in which GFDL AM3's aerosol-driven solar dimming over East Asia has been verified against observational estimates (Persad et al. 2014). The initial simulation year (1980) is then excluded from analysis to eliminate discontinuities associated with imposing the idealized forcing, and the idealized forcing signal is calculated as the difference between the 1981–2000 average of the perturbed simulation and the ALL simulation. In the idealized forcing cases a single simulation, rather than an ensemble, is used. The construction and goal of each idealized forcing simulation is schematically depicted in Fig. 1.

a. Pure dimming

A purely scattering optical depth (i.e., with an effective single scattering albedo of 1), scaled to reduce surface shortwave radiation (SSR) by a level comparable to that produced by realistic aerosol, is imposed onto the ALL control. The scattering optical depth τ_d within each model layer of pathlength or depth Δz is calculated according to the layer average pressure p via the following equation, which approximates the vertical structure of the realistic aerosol perturbation:

$$\tau_d(p) = \begin{cases} \Delta z\, \alpha_d \left(\dfrac{p-150}{p_0}\right)^{\beta_d}, & \text{for} \quad p \geq 150\,\text{mb} \\ 0, & \text{for} \quad p < 150\,\text{mb} \end{cases},$$

where $\alpha_d = 0.117\,\text{km}^{-1}$ is a scaling constant designed to achieve a comparable magnitude of regional and summertime (June–August) mean all-sky surface shortwave reduction (i.e., dimming) as realistic aerosol, and $\beta_d = 2$ is a decay rate designed to approximate the vertical structure of the realistic aerosol perturbation.

The difference between the above perturbed simulation and the ALL simulation, averaged over 1981–2000, is hereafter referred to as the "pure dimming" signal and isolates the effects of surface dimming from that of atmospheric heating. The primary role of the pure dimming signal, in the context of this analysis, is to allow us to analyze how surface dimming from an absorber affects the overall response to the absorption. However, it can also be thought of as simulating the behavior of dimming from purely scattering aerosols.

b. Pure heating

An idealization of the atmospheric shortwave heating profile from realistic aerosol is imposed onto the ALL simulation. The idealized shortwave heating rate Tdt_{sw}

is calculated at each pressure level p to mimic the bottom-heavy vertical structure and magnitude of that produced by the realistic regional aerosol and takes the exponential form:

$$Tdt_{\mathrm{sw}}(p) = \alpha_h \frac{S}{\overline{S}} e^{\beta_h p/p_0},$$

where $\alpha_h = 1\,\mathrm{K\,s^{-1}}$ is a scaling constant designed to give a heating rate magnitude comparable to the realistic regional aerosol perturbation, and $\beta_h = 1$ is a decay rate designed to approximate the vertical structure of the realistic aerosol perturbation. The variable S is the time- and grid-varying solar flux in watts per meter squared, $\overline{S}$ is the regionally and annually averaged solar flux in watts per meter squared, and $p_0 = 1000\,\mathrm{mb}$ ($1\,\mathrm{mb} = 1\,\mathrm{hPa}$) is the surface reference pressure. The perturbation heating rate is imposed at every time step but is scaled according to diurnal and seasonal changes in solar zenith angle and solar flux, as reflected in the $S/\overline{S}$ term. The resulting regional- and seasonal-mean heating rate are discussed and compared with that produced by realistic aerosol in section 4c.

The difference between the above perturbed simulation and the ALL simulation, averaged over 1981–2000, is hereafter referred to as the "pure heating" signal and isolates the impact of atmospheric heating in the absence of any associated surface dimming. In conjunction with the pure dimming signal, this allows us to quantify the degree to which the overall response to an aerosol population that contains absorption is influenced by its atmospheric heating versus its surface dimming.

c. Pure absorption

A purely absorbing optical depth (i.e., with an effective single scattering albedo of 0) is scaled to produce surface dimming comparable to that seen in the realistic aerosol case. As in the pure dimming case, the absorbing optical depth τ_a within each model layer of depth Δz is calculated according to the layer average pressure p via the following equation, which approximates the vertical structure of the realistic regional aerosol perturbation:

$$\tau_\alpha(p) = \begin{cases} \Delta z\,\alpha_a \left(\dfrac{p-150}{p_0}\right)^{\beta_a}, & \text{for} \quad p \geq 150\,\mathrm{mb} \\ 0, & \text{for} \quad p < 150\,\mathrm{mb} \end{cases},$$

where $\alpha_a = 0.019\,\mathrm{km^{-1}}$ is the magnitude scaling constant, and $\beta_a = 2$ is the vertical decay rate (identical to the pure-dimming vertical decay rate β_d), both designed to approximate the realistic aerosol perturbation. The resulting shortwave heating rate is compared with that produced by the realistic aerosol and pure heating cases in section 4c.

The difference between the above perturbed simulation and the ALL simulation, averaged over 1981–2000, is hereafter referred to as the "pure absorption" signal. An absorbing aerosol will both heat the atmosphere by trapping shortwave radiation therein (as in the pure heating simulation) and dim the surface by attenuating shortwave radiation aloft (as in the pure dimming simulation). This final simulation allows us to capture a radiative idealization of both the surface and atmospheric effects of absorbing aerosols acting in combination (resulting distinctions from the effects of realistic East Asian black carbon emissions are discussed in section 4d).

The three idealized forcing simulations are designed to be intercomparable. Comparison of all three idealized perturbation simulations allows a full decomposition of how absorption's atmospheric and surface radiative perturbations operate in isolation and in tandem. Secondarily, comparison of the pure dimming and pure absorption signals allows quantification of how the response to dimming driven by absorbing versus scattering aerosols differs. Because of the radiative nature of the idealized perturbations' parameterizations, microphysical indirect effects—such as the Twomey (1977) and Albrecht (1989) effects—are not excited directly by the idealized forcing perturbations. All cloud changes in the idealized forcing simulations will thus be thermodynamically [including semidirect aerosol effects (e.g., Hansen et al. 1997)] or dynamically driven, although they may produce additional feedbacks on the circulation (Guo et al. 2015).

The realistic aerosol signal is primarily used to determine reasonable radiative perturbations for the idealized forcing simulations and should not be construed as directly comparable to the three idealized forcing signals. Because of its formulation differences with the idealized forcing simulations, such as the presence of microphysical aerosol indirect effects in the former case and differences in the control climate and spatiotemporal distribution of forcing, precise correspondence between the realistic aerosol case and the three idealized forcing signals is not expected. However, it is informative to view the realistic aerosol case, which contains both scattering and absorbing aerosols, as some combination of the pure absorption and the pure dimming signals (with the addition of microphysical aerosol indirect effects).

All analysis is done on the mean of June, July, and August (JJA), which captures the main mei-yu–baiu period of EASM rainfall (e.g., Tao and Chen 1987). Statistical significance is determined using the Student's t test, adjusting for the autocorrelation of consecutive years of data as in Santer et al. (2000).

3. Results

a. Radiative effects of realistic and idealized aerosols

Table 1 summarizes the regional-mean clear-sky and all-sky surface dimming and atmospheric absorption produced by the various model perturbations, as well as their regional-mean top-of-the-atmosphere effective radiative forcing [defined as the net downward radiative flux at the top of the atmosphere after atmospheric and land-surface conditions have been allowed to equilibrate to the perturbation (Myhre et al. 2013)]. Clear-sky values are calculated by the model's radiative transfer code with clouds removed. Microphysical aerosol indirect effects are present in the realistic aerosol case and may influence differences between clear-sky and all-sky (i.e., cloud permitting) values. In the idealized forcing simulations, because microphysical aerosol indirect effects are not in operation, differences between all-sky and clear-sky values are explained by either 1) thermodynamically or dynamically driven cloud changes that reinforce or counteract the aerosols' radiative interactions (see Fig. 6b) or 2) differences due to cloud masking in the amount of radiation with which the aerosol is interacting in the clear-sky versus all-sky calculation.

The presence of realistic regional aerosols reduces the solar radiation incident at the surface over East Asia by $\Delta SSR_{all} = -14.3\,W\,m^{-2}$ in the 1981–2000 mean, consistent with the finding of others in both models and observations (e.g., Norris and Wild 2009; Dwyer et al. 2010; Allen et al. 2013). Note that, because our simulations only include aerosol emissions within China, they contain less aerosol over East Asia than the models and observations in the above-referenced work, which include aerosols transported from both local and remote sources. The surface dimming signal is evident both in the presence and in the absence of cloud cover (i.e., ΔSSR_{all} and ΔSSR_{clr} in Table 1). It is driven almost equally by scattering and by absorption of shortwave radiation by aerosols within the atmospheric column [consistent with the findings of Persad et al. (2014)], evident via comparison of ΔSSR_{all} and ΔAbs_{all} in Table 1.

The similarity of the clear-sky and all-sky SSR changes in response to realistic aerosol should not be interpreted as an absence of aerosol–cloud interactions. Aerosol indirect effects operate in the realistic aerosol case and result in a 97% increase in cloud droplet number concentration (not shown) through the activation of aerosols as cloud condensation nuclei, thus increasing the shortwave cloud reflectivity (Donner et al. 2011). Simultaneously, the presence of cloud above aerosol masks the interaction of the underlying scattering and absorbing aerosol with downwelling shortwave radiation. With the removal of cloud in the clear-sky calculation, these factors tend to compensate for one another, resulting in a net minimal difference in surface shortwave radiation between the clear-sky and all-sky calculations.

TABLE 1. Regional-mean radiative perturbations ($W\,m^{-2}$) over East Asia (22.5°–40°N, 100°–122.5°E) are shown for each of the four simulations for the changes in all- and clear-sky surface shortwave radiation (ΔSSR_{all} and ΔSSR_{clr}, respectively; positive downward), all- and clear-sky atmospheric shortwave absorption (ΔAbs_{all} and ΔAbs_{clr}, respectively; positive into the atmosphere), and regional all- and clear-sky top-of-the-atmosphere effective radiative forcing (ΔF_{all}^{TOA} and ΔF_{clr}^{TOA}, respectively; positive downward). Asterisks indicate perturbations that are not significant at the 95% confidence level.

	Realistic aerosol	Pure dimming	Pure heating	Pure absorption
ΔSSR_{all}	−14.3	−18.6	−0.19*	−14.6
ΔSSR_{clr}	−13.5	−29.0	0.04*	−16.2
ΔAbs_{all}	6.87	−1.35	−0.49*	17.3
ΔAbs_{clr}	7.29	−2.76	0.10*	19.1
ΔF_{all}^{TOA}	−6.75	−19.8	2.04*	6.57
ΔF_{clr}^{TOA}	−4.35	−27.4	0.09*	6.13

The idealized pure dimming simulation—designed primarily to isolate the surface effects of atmospheric absorption but also capturing the response to purely scattering-driven dimming—produces an all-sky SSR reduction of $\Delta SSR_{all} = -18.6\,W\,m^{-2}$. The difference between the clear-sky and all-sky SSR reduction can be largely explained by climatological cloud masking, as each constitutes a comparable fractional reduction in its respective control SSR budget (10% in the clear-sky case and 9% in the all-sky case). Cloud amount also decreases by approximately 3% (see Table 3), which appears to be consistent with the smaller all-sky SSR reduction relative to the clear-sky SSR reduction. However, this is the result of a decrease in middle and high cloud and an increase in low cloud (see Fig. 6b), making the overall shortwave effects of the vertically integrated cloud change difficult to determine.

Because the pure heating simulation—designed to isolate the atmospheric effects of aerosol absorption—has a heating rate rather than an optical depth imposed, the SSR and absorption perturbations are deliberately minimal in that simulation. As evinced by the difference between the clear-sky and all-sky values (Table 1), they are primarily driven by cloud changes that are consistent with the overall circulation response discussed in section 4c.

Although the absorption optical depth in the pure absorption case—designed to probe the combined surface and atmospheric effects of purely absorption-driven dimming—is comparable to that of the realistic

TABLE 2. Regional-mean surface energy flux changes ($W m^{-2}$) over East Asia (22.5°–40°N, 100°–122.5°E) are shown for each of the four simulations, as well as the residual of all surface energy balance adjustment. All values are given as downward positive. Asterisks indicate perturbations that are not significant at the 95% confidence level.

	Realistic aerosol	Pure dimming	Pure heating	Pure absorption
$\Delta SW_{\downarrow}$	−14.3	−18.6	−0.19*	−14.6
$\Delta SW_{\uparrow}$	2.09	2.64	0.03*	2.37
$\Delta LW_{\downarrow}$	−0.62	−3.22	−0.12*	−0.43*
$\Delta LW_{\uparrow}$	1.16	4.45	−0.09*	2.36
$\Delta SH_{\uparrow}$	3.23	5.30	2.00*	5.71
$\Delta LH_{\uparrow}$	7.13	8.95	−1.82	4.14
Residual	−1.31	−0.48	−0.19	−0.45

aerosol case (see section 2), it produces a larger amount of absorption due to the absence of aerosol scattering and aerosol indirect effects, which might otherwise attenuate the shortwave radiation before it reaches an absorber. The increased absorption ($\Delta Abs_{all} = 17.3\,W\,m^{-2}$) produces a corresponding reduction in SSR ($\Delta SSR_{all} = -14.6\,W\,m^{-2}$). The atmospheric absorption is larger than the SSR reduction partly due to additional absorption produced by shortwave radiation reflected from the surface, which is not counted in the downward-incident SSR change.

b. Surface energy balance response

On seasonal-mean (and longer) time scales the land-surface energy balance is constrained to maintain approximate equilibrium due to the low effective heat capacity of the land surface. As a result, the reduction in downwelling surface shortwave flux $\Delta SW_{\downarrow}$ caused by the scattering and/or absorption in the three cases that contain dimming (realistic aerosol, pure dimming, and pure absorption) must be compensated for by changes in the other surface energy balance terms: reflected upwelling shortwave flux $\Delta SW_{\uparrow}$, net longwave flux $\Delta LW_{\downarrow} + \Delta LW_{\uparrow}$, sensible heat flux $\Delta SH_{\uparrow}$, and latent heat flux $\Delta LH_{\uparrow}$; that is, $\Delta F_s = (\Delta SW_{\downarrow} + \Delta SW_{\uparrow}) + (\Delta LW_{\downarrow} + \Delta LW_{\uparrow}) + \Delta SH_{\uparrow} + \Delta LH_{\uparrow} = 0$ for all values downwelling positive.

These changes are shown in Table 2. Slight residuals in the surface energy balance can be attributed to the long adjustment times induced by the deep soil moisture in GFDL AM3's land model (Donner et al. 2011). Surface albedo does not change significantly between the simulations, remaining at $\alpha \approx 0.16$. Consequently, the change in upwelling shortwave radiation is a direct result of the change in downwelling shortwave radiation, and $\Delta SW_{\uparrow} \approx 0.16\Delta SW_{\downarrow}$ in all four cases. The surface upwelling longwave flux maintains a quartic relationship with surface temperature, according to the Stefan–Boltzmann law, while sensible and latent heat flux are controlled by temperature and moisture gradients between the surface and near-surface atmosphere, as well as surface wind speed.

The idealized forcing simulations indicate that the response of the surface energy balance to the reduction in SSR is dependent on whether the surface dimming is accompanied by atmospheric heating. When the dimming occurs without atmospheric heating (i.e., the pure dimming case, also interpretable as dimming from a scattering aerosol), the change in latent heat flux balances 48% of the dimming ($\Delta SW_{\downarrow}$), while the change in sensible heat flux accounts for 28% and the change in net longwave flux accounts for only 6.6%. Where the dimming is accompanied by strong atmospheric heating (i.e., the pure absorption case), however, the contribution from the change in sensible heat flux exceeds that from the change in latent heat flux; reduced sensible heat flux accounts for the plurality (39%) of the surface energy balance's reequilibration to the dimming ($\Delta SW_{\downarrow}$), while reductions in outgoing latent heat and net longwave flux account for the remaining 28% and 13%, respectively. Note that upwelling shortwave flux contributes the remaining energy balance equilibration in both cases but is a simple albedo scaling of the change in downwelling shortwave. Because there is not an explicit radiative perturbation in the pure heating simulation, the perturbation to its surface energy balance cannot be construed as a response to $\Delta SW_{\downarrow}$. Indeed, radiative fluxes remain relatively unperturbed. However, sensible heat flux decreases, while latent heat flux increases by a similar amount (note that all values are given as downward positive).

The partitioning of the surface energy balance response to dimming from realistic aerosol, although it is driven half by atmospheric absorption (Table 1), is almost identical to the pure dimming case. The reduction in latent heat balances 49% of the dimming, although outgoing sensible heat and longwave flux also decrease, balancing 23% and 3.8% of the dimming, respectively. This suggests that the larger sensible heat flux response seen in the pure absorption case than in the pure dimming case requires a dominating absorption contribution to the dimming. We explore the mechanisms behind the relative behavior of the sensible versus latent heat flux response to dimming in section 4b.

c. Impact on EASM strength

As the primary mechanism for regional rainfall in East Asia, monsoon strength is frequently quantified to the first order by the regional mean precipitation (e.g., Lu et al. 2006; Bollasina et al. 2011). Because of their role in supporting this monsoonal precipitation, convective activity and the land–sea thermal contrast are generally used to

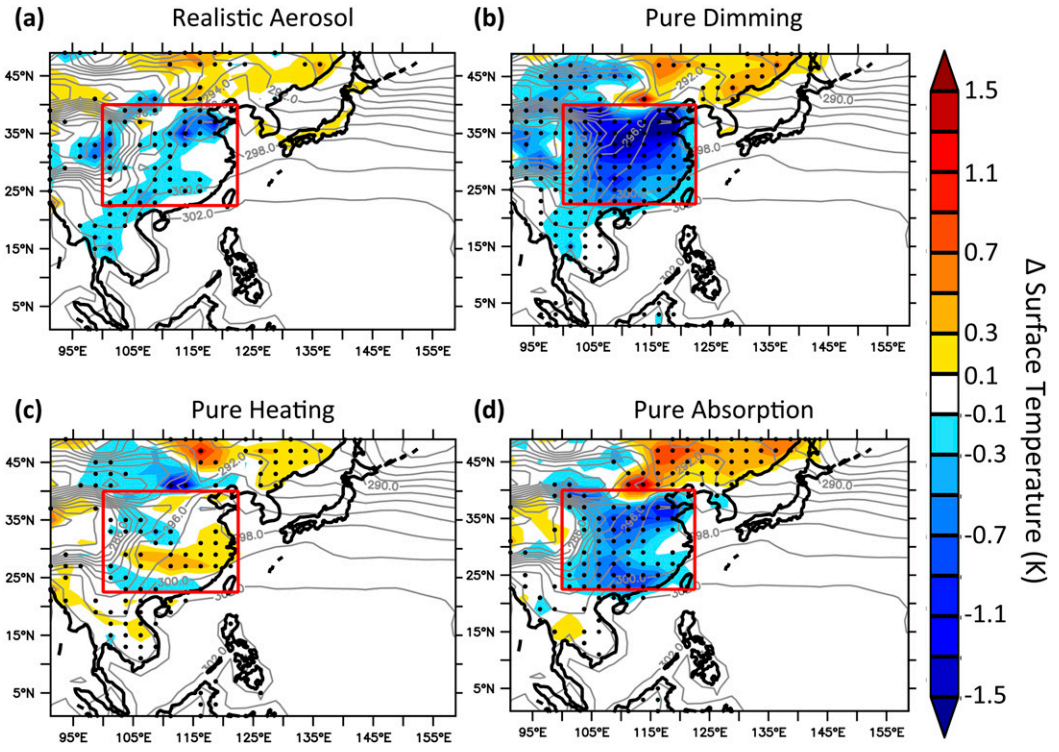

FIG. 2. The surface temperature response (shading; K) to (a) historical regional aerosols, (b) a purely scattering aerosol optical depth, (c) idealized atmospheric heating, and (d) a purely absorbing aerosol optical depth. Climatological values are shown in gray contours, and coastal outlines are shown in black. The red box delineates East Asia (22.5°–40°N, 100°–122.5°E), over which idealized perturbations are imposed and regional means are calculated. Stippling indicates responses that are significant at the 95% confidence level.

evaluate the overall monsoon circulation strength (e.g., Wang et al. 2008; Dai et al. 2013). Because sea surface temperature is fixed and atmospheric moisture changes are negligible (<0.1%) compared to temperature changes (and equivalent potential temperature gradients—one measure of thermal contrast—therefore follow temperature gradients) across all four signals, land–sea thermal contrast change is robustly captured by change in land-surface temperature. Consequently, we use these standard parameters to characterize qualitative changes in the EASM strength: land–sea thermal contrast (i.e., land-surface temperature; shown in Fig. 2), onshore flow (i.e., 850-mb winds; shown in Fig. 3), atmospheric ascent (i.e., 500-mb vertical velocity in pressure coordinates ω_{500}; shown in Fig. 4) over land, and, ultimately, precipitation (Fig. 5). We also summarize the overall monsoon strength quantitatively using the total precipitation averaged over East Asia and the 850-mb wind speed averaged over the East Asian monsoon sector (10°–40°N, 110°–150°E) as defined by Li and Zeng (2002) for quantifying EASM variability (Table 3).

The realistic aerosol signal indicates that historical regional anthropogenic aerosol emissions have reduced the strength of the EASM, consistent with past research (e.g., Song et al. 2014; Wang et al. 2015). Although atmospheric absorption in the realistic aerosol case results in substantial shortwave heating throughout the lower atmosphere (section 4c), the overall radiative effects of the anthropogenic aerosol loading reduces the regional-mean land-surface temperature (Fig. 2a). Decreasing land–sea contrast reduces onshore low-level winds (Fig. 3a). The land-surface cooling also drives a 6% reduction in the climatologically ascending motion (i.e., $\omega_{500} < 0$) over the land surface, although some subregional meridional variation exists (Fig. 4a). This overall counteraction of EASM circulation causes a 6% reduction in regional-mean precipitation (Table 3 and Fig. 5a).

The idealized forcing simulations illuminate how the different aerosol radiative components contribute to reduced EASM strength. Solar dimming in isolation (pure dimming) decreases EASM strength by reducing the climatological land–sea thermal contrast (Fig. 2b), consistent with previous studies (e.g., Guo et al. 2013; Wang et al. 2015). The deficit in surface shortwave energy cools the land surface and lower troposphere

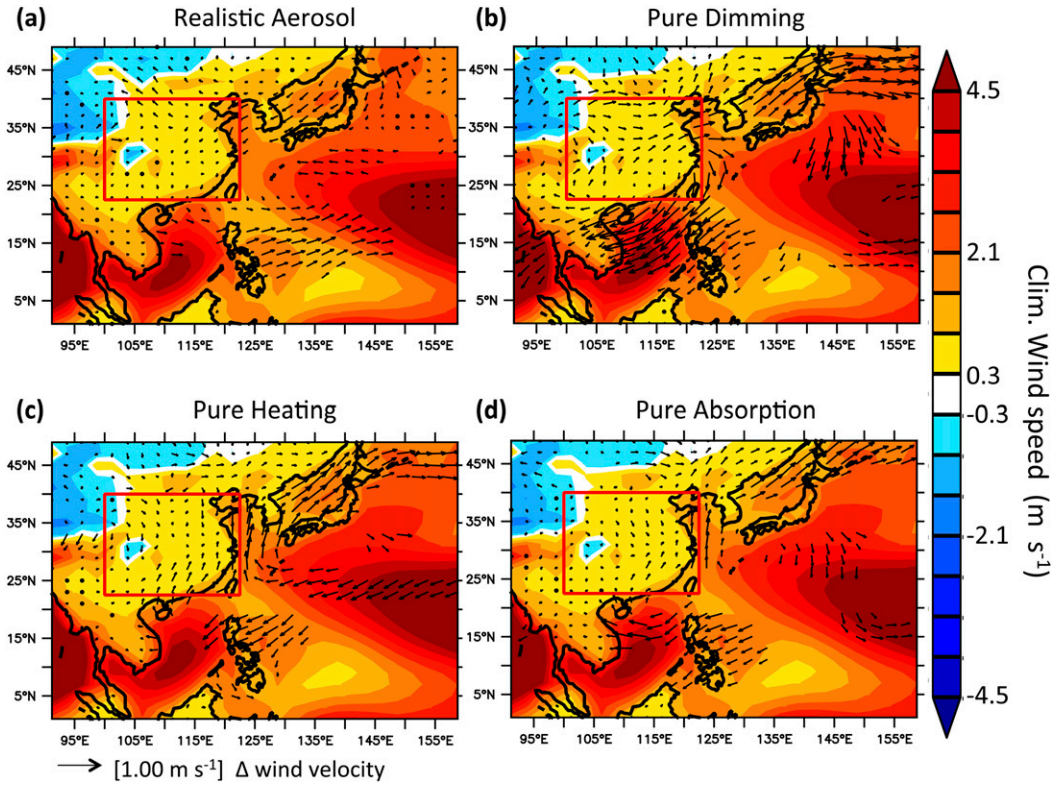

FIG. 3. The change in 850-mb wind velocity (vectors; m s^{-1}) in response to (a) historical regional aerosols, (b) a purely scattering aerosol optical depth, (c) idealized atmospheric heating, and (d) a purely absorbing aerosol optical depth. Wind vectors are only shown for changes that are significant at the 95% confidence level. Climatological wind speeds (m s^{-1}) are shaded, with sign convention following meridional wind direction (southerly positive). Coastal outlines are shown in black. The red box delineates East Asia (22.5°–40°N, 100°–122.5°E), over which idealized perturbations are imposed and regional means are calculated.

(Fig. 6c), weakening onshore low-level winds (Fig. 3b and Table 3). This coincides with a 25% decrease in atmospheric ascent (Fig. 4b and Table 3) and an 8.0% reduction in regional-mean precipitation (Table 3 and Fig. 5b).

Conversely, pure atmospheric heating in the absence of any surface shortwave perturbation (pure heating) enhances EASM circulation in our model. The surface temperature response to the atmospheric heating (Table 3 and Fig. 2c) is minimal, as are changes in tropospheric temperature (Fig. 6c). However, the imposed atmospheric shortwave heating increases ascending motion over the land surface by 37% (Fig. 4c and Table 3). This drives lower-level convergence that weakly increases the 850-mb flow of moisture-laden air from the surrounding ocean area (Table 3 and Fig. 3c), increasing regional-mean precipitation by 6.3% (Table 3 and Fig. 5c).

Both the solar dimming and the atmospheric heating are active in the pure absorption case, and the EASM circulation response is correspondingly a combination of the effects of the two components. While the atmospheric absorption drives an atmospheric shortwave heating rate comparable to the pure heating case (section 2), the attenuation of this shortwave radiation within the atmosphere results in a substantial reduction in surface solar radiation (Table 1) that drives surface cooling (Fig. 2d) and lower-tropospheric cooling (Fig. 6c). The atmospheric heating enhances ascending motion by 21% (Fig. 4d and Table 3), but the solar dimming simultaneously cools the land surface (Table 3). Although this does reduce onshore low-level winds (Fig. 3d), it does so by less than the pure dimming case (Table 3). The precipitation response is small (Table 3 and Fig. 5d) but net negative (−1.6%), an outcome that will be further discussed in section 4.

d. *Moisture budget response*

The surface energy balance and monsoon circulation responses combine in determining the overall moisture budget response, as characterized by the response in precipitation ΔP, evaporation ΔE (proportional to the

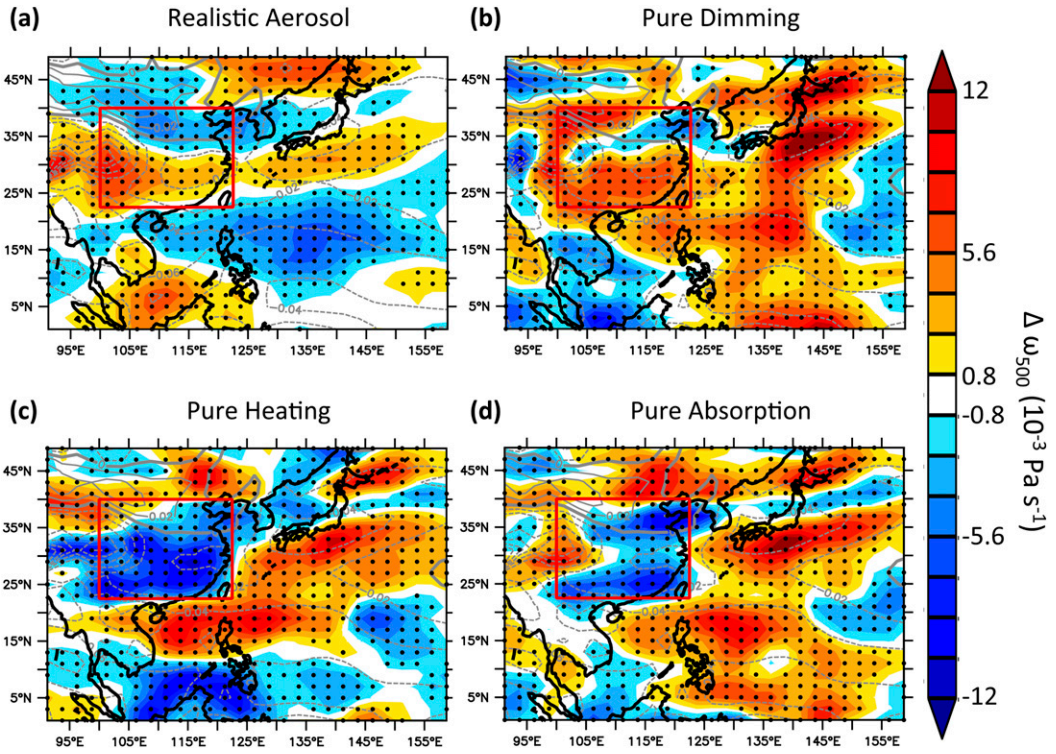

FIG. 4. The midtropospheric (500 mb) vertical pressure velocity ω response (shading; 10^{-3} Pa s^{-1}) to (a) historical regional aerosols, (b) a purely scattering aerosol optical depth, (c) idealized atmospheric heating, and (d) a purely absorbing aerosol optical depth. Climatological values (Pa s^{-1}) are shown in gray contours, and coastal outlines are shown in black. The red box delineates East Asia (22.5°–40°N, 100°–122.5°E), over which idealized perturbations are imposed and regional means are calculated. Stippling indicates responses that are significant at the 95% confidence level.

change in surface latent heat flux), and the moisture convergence necessary to balance the two $\Delta(P - E)$. Changes in atmospheric moisture content are negligible (<0.1%) and, therefore, may be robustly neglected (Fig. 6d). East Asian summertime climate is characterized by climatological moisture convergence ($P > E$).

Table 4 shows the moisture budget values for each of the four perturbations. In the presence of realistic aerosol or idealized pure dimming, moisture convergence decreases (consistent with the counteraction of monsoonal flow discussed in section 3c), as the reduction in P exceeds the reduction in E. In the pure heating simulation, conversely, moisture convergence increases, as increased P outweighs increased E. The pure absorption case shows a counterbalancing of these two effects; although both P and E decrease as in the realistic aerosol and pure dimming case, moisture convergence still increases, as the P reduction is smaller than the E reduction. The differences in ΔP, ΔE, and $\Delta(P - E)$ between the pure absorption and pure dimming cases (8.99, 4.81, and 4.18 W m^{-2}, respectively) are of the same sign as the values in the pure heating case and of comparable magnitude (Table 4), suggesting that the pure absorption behavior can be interpreted as a superposition of the pure dimming and pure heating cases. Energy balance constraints provide an investigation of this outcome, discussed in section 4a.

4. Discussion

a. *An energetic rationalization of absorption's effect on the EASM*

Our results demonstrate that the EASM response to realistic regional aerosol emissions is dominated by the suppressing effect of their surface solar dimming, even in the presence of strong shortwave atmospheric absorption by the aerosols. An interesting first-order question then is whether the EASM response, as summarized in the regional-mean precipitation change, is at all sensitive to the presence of the atmospheric heating or is simply a response to the surface solar dimming—a question that can be addressed via comparison of the results of our idealized forcing simulations.

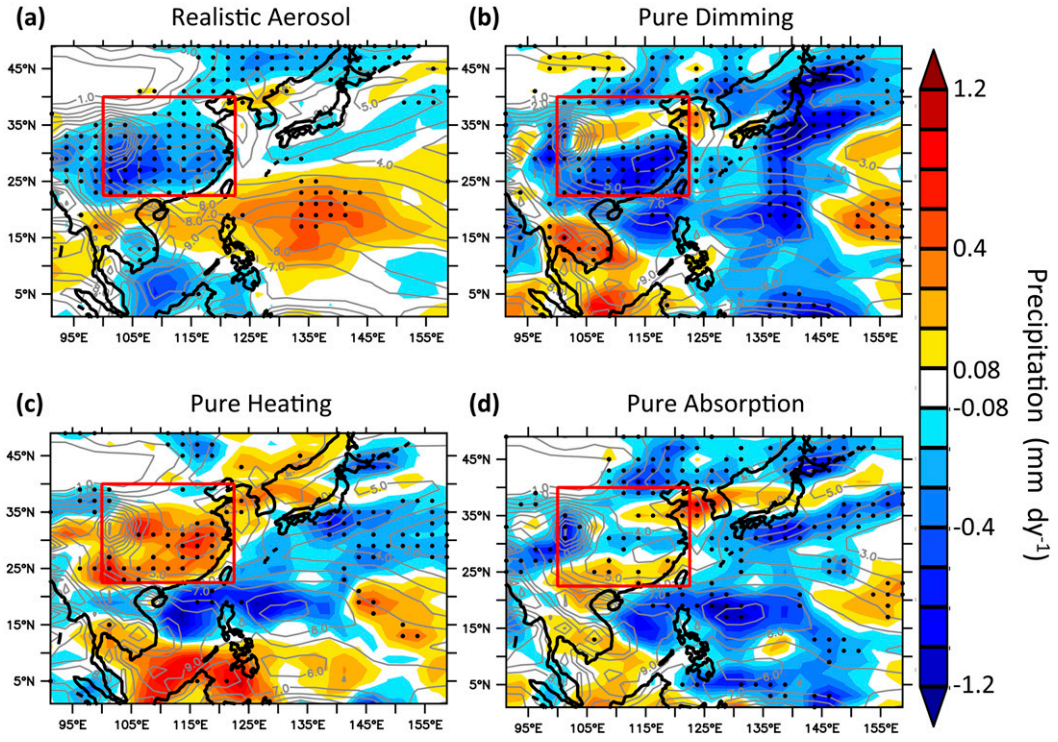

FIG. 5. The change in precipitation (shading; mm day^{-1}) in response to (a) realistic historical aerosols, (b) a purely scattering aerosol optical depth from historical aerosol, (c) idealized atmospheric heating, and (d) a purely absorbing aerosol optical depth. Climatological values (mm day^{-1}) are shown in gray contours, and coastal outlines are shown in black. The red box delineates East Asia (22.5°–40°N, 100°–122.5°E), over which idealized perturbations are imposed and regional means are calculated. Stippling indicates changes that are significant at the 95% confidence level.

Because of variations in how the imposed perturbation translates into a surface radiative effect in each of our simulations (section 2), the surface dimming values across the simulations that contain an explicit radiative perturbation (i.e., realistic aerosol, pure dimming, and pure absorption) are not identical. To understand how the response to a given amount of surface dimming depends on the source of that dimming, we normalize out the small differences in the amount of surface dimming across our simulations to allow direct comparison. We refer to this approach as ''per unit dimming'' in the remainder of this work and calculate it by dividing the response of interest (e.g., ΔP) by the change in surface shortwave radiation ΔSSR_{all} for a given simulation.

The precipitation response does not scale linearly with SSR reduction across the perturbations. The precipitation change per unit dimming in the pure dimming case is 3–4 times larger than that in the pure absorption case (Table 4), indicating that the atmospheric effects of the aerosol absorption have a damping effect on the precipitation response to the surface dimming. Pure heating on its own has little to no effect on the surface shortwave radiation or surface temperature but increases precipitation substantially, hinting that other processes besides land–sea contrast can influence EASM strength. The smaller precipitation reduction under pure absorption than under pure dimming, thus, is

TABLE 3. Regional-mean responses over East Asia (22.5°–40°N, 100°–122.5°E) are shown for each of the four perturbations. The change in column-integrated cloud amount (ΔCloud), given in percent of grid cloud coverage; the change in surface and near-surface air temperature (ΔT_s and ΔT_a, respectively; K); the change in precipitation ($\Delta P/P$), given in percent of climatological values; and the change in vertical pressure velocity at 500 mb ($\Delta\omega_{500}$; 10^{-3} Pa s^{-1}). The change in 850-mb wind speed (ΔV_{850}) is averaged over the East Asian monsoon sector (10°–40°N, 100°–150° E) following Li and Zeng (2002). Asterisks indicate perturbations that are not significant at the 95% confidence level.

	Realistic aerosol	Pure dimming	Pure heating	Pure absorption
ΔCloud	−0.28*	−0.87	0.41	1.14
ΔT_s	−0.18	−0.74	0.01*	−0.38
ΔT_a	−0.08	−0.69	0.04	−0.33
$\Delta P/P$	−6.0	−8.0	6.3	−1.6
$\Delta\omega_{500}$	1.0	3.5	−5.2	−3.0
ΔV_{850}	−0.01*	−0.11	0.04*	−0.08

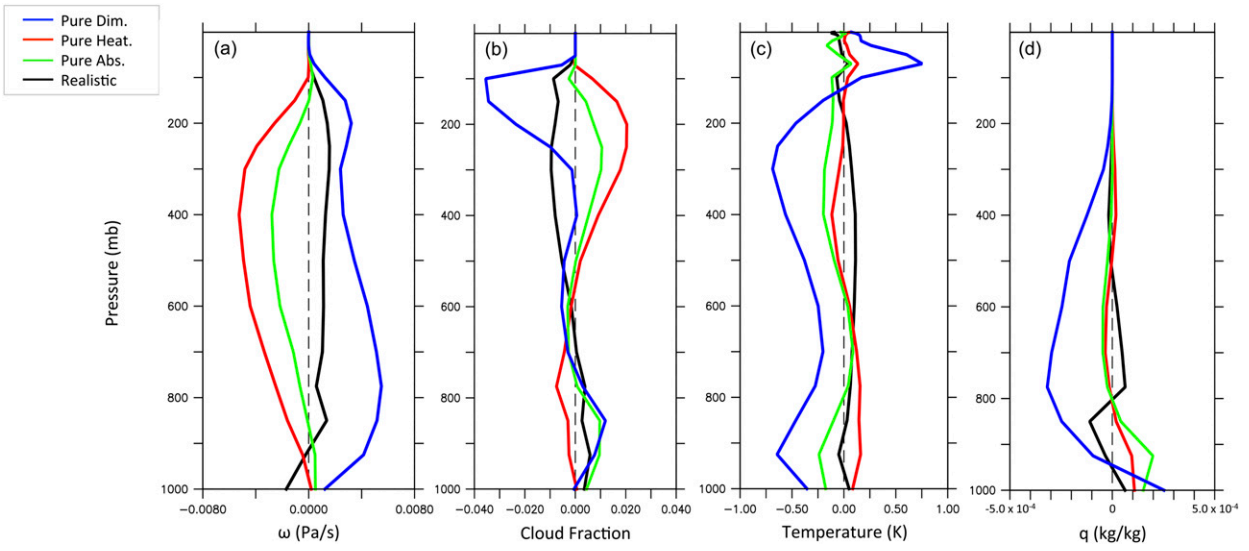

FIG. 6. Vertical profiles of changes in (a) pressure velocity ω, (b) cloud fraction, (c) temperature, and (d) moisture mixing ratio or specific humidity q averaged over East Asia (22.5°–40°N, 100°–122.5°E) are shown for the four simulations.

not achieved via a modulation of the land–sea surface temperature contrast that drives the circulation decrease under pure dimming; another mechanism must be invoked.

We turn to the atmospheric energy and moisture budgets to seek guidance on how atmospheric heating modulates the precipitation reduction from absorbing aerosols. First, we use the atmospheric moist static energy (MSE) budget to establish a relationship between the atmospheric energy input by each perturbation and the vertical motion induced. Second, we use the moisture budget to establish a relationship between vertical motion and precipitation response.

The MSE budget dictates that the net energy input into the atmospheric column must be balanced by the divergent moist static energy transport. In monsoonal systems, this balance may be approximated as follows (Chou and Neelin 2003):

$$\left\langle \frac{\delta h}{\delta t} \right\rangle (\approx 0) = F_{\text{net}} - \langle \mathbf{v} \cdot \nabla h \rangle - \left\langle \omega \frac{\delta h}{\delta p} \right\rangle. \qquad (1)$$

The seasonal mean vertical integral $\langle X \rangle$ of the time variation of moist static energy ($h = c_p T + gz + L_v q$, where c_p is specific heat, T is atmospheric temperature, g is gravity, z is geopotential height, L_v is the latent heat of vaporization, and q is specific humidity) can be approximated as 0, since the atmosphere's capacity for energy storage is minimal. Thus, the net energy input into the atmospheric column ($F_{\text{net}} = \text{SW}^{\text{sfc}}_{\uparrow} + \text{SW}^{\text{sfc}}_{\downarrow} + \text{SW}^{\text{TOA}}_{\downarrow} + \text{SW}^{\text{TOA}}_{\uparrow} + \text{OLR} + \text{LW}^{\text{sfc}}_{\downarrow} + \text{LW}^{\text{sfc}}_{\uparrow} + \text{SH}_{\uparrow} + \text{LH}_{\uparrow}$, for all values positive into the atmosphere) must be roughly balanced by the horizontal advection $\langle \mathbf{v} \cdot \nabla h \rangle$ and vertical advection within the atmospheric column $\omega \langle \delta h / \delta p \rangle$ of moist static energy.

The horizontal advection term generally can be neglected under the approximately radiative–convective equilibrium conditions of the summer monsoon (Neelin and Held 1987). Thus, Eq. (1) can be simplified as $F_{\text{net}} \approx \omega \langle \delta h / \delta p \rangle$. It can be further assumed that $\langle \delta h / \delta p \rangle < 0$ in the troposphere and will be dominantly controlled by moist convection[1] (e.g., Chen and Bordoni 2014), yielding the simplified proportionality $F_{\text{net}} \propto -\langle \omega \rangle$.

The above relationship can then be used to understand the dynamical response to our imposed perturbations in the adjustment sense: $\Delta F_{\text{net}} \propto -\Delta \langle \omega \rangle$. Then, because the surface energy balance will rapidly equilibrate to zero over land $F_s \approx 0$, the change in net energy input into the atmospheric column reduces to $\Delta F_{\text{net}} = \Delta F_s + (\Delta \text{SW}^{\text{TOA}}_{\downarrow} + \Delta \text{SW}^{\text{TOA}}_{\uparrow} + \Delta \text{OLR}) = 0 + \Delta F^{\text{TOA}}$, where ΔF^{TOA} is the change in top-of-the-atmosphere flux. The proportionality thus can be further approximated as $\Delta F^{\text{TOA}} \propto -\Delta \langle \omega \rangle$. Note that, in fixed SST simulations such as ours, the equilibrium change in top-of-the-atmosphere flux is equivalent to the top-of-the-atmosphere effective radiative forcing (ΔF^{TOA} in Table 1).

The proportionality, given by $\Delta F^{\text{TOA}} \propto -\Delta \langle \omega \rangle$, indicates that a change in the vertical integral of the

[1] The $\langle \delta h / \delta p \rangle$ changes by <1% in response to the idealized forcings (not shown).

TABLE 4. The moisture budget averaged over East Asia (22.5°–40°N, 100°–122.5°E) is shown for each of the four perturbations, with changes (W m^{-2}) in precipitation (ΔP), evaporation (ΔE; cf. $\Delta LH_{\uparrow}$ in Table 2), and moisture convergence [$\Delta(P - E)$] values. Per unit dimming values (i.e., divided by $-\Delta SSR_{all}$ for the corresponding simulation) are shown in parentheses [W m^{-2} (W m^{-2})$^{-1}$] for all but pure heating, which does not contain imposed surface dimming.

	Realistic aerosol	Pure dimming	Pure heating	Pure absorption
ΔP	−9.35 (−0.65)	−11.17 (−0.61)	8.77	−2.18 (−0.15)
ΔE	−7.13 (−0.50)	−8.95 (−0.49)	1.82	−4.14 (−0.28)
$\Delta(P - E)$	−2.22 (−0.16)	−2.22 (−0.12)	6.95	1.96 (0.13)

vertical pressure velocity ω caused by an aerosol perturbation will be proportional to its TOA effective radiative forcing [i.e., a positive (negative) forcing will induce a net column-integrated ascending (subsiding) perturbation to vertical motion in the atmosphere]. Comparison of the vertical profiles of ω (Fig. 6a) and ΔF^{TOA} (Table 1) shows that this relationship holds for all three cases with a closed energy budget (i.e., realistic aerosol, pure dimming, and pure absorption), indicating that the simplified proportionality is applicable to this regime. Ascending motion must increase under pure absorption's positive TOA forcing and decrease under pure scattering's negative TOA forcing.

Note that, because the pure heating case involves the artificial imposition of a shortwave heating rate, the above framework will not strictly hold, although the relative signs of $\Delta\omega$ and ΔF^{TOA} are still consistent. In this case, the imposed shortwave heating rate should be considered an additional input of energy into the atmosphere, which would need to be accounted for in the F_{net} term. Because it is artificially imposed rather than induced by an explicit radiative perturbation, unlike the shortwave heating in pure absorption, it is otherwise not directly reflected in the F_s or F^{TOA} terms.

The vertically integrated moisture budget then connects this vertical motion to the regional precipitation. To the first order, the moisture budget dictates that any change in moisture convergence will be proportional to the change in the integrated vertical moisture advection; that is, $\Delta(P - E) \propto \Delta(-\omega\langle\delta q/\delta p\rangle)$, again assuming changes in horizontal advection will be negligible compared to changes in vertical advection under summer monsoon conditions[2] (e.g., Chou and Neelin 2003). Changes in $\delta q/\delta p$ are small relative to changes in ω (percent changes compared to climatological conditions are on the order of 10%–20% for ω versus 0%–2% for $\delta q/\delta p$), so the proportionality can be approximated as $\Delta(P - E) \propto -\Delta\langle\omega\rangle$. Therefore, the enhanced ascending motion under pure absorption's positive ΔF^{TOA} constrains the moisture convergence to increase [$\Delta(P - E) > 0$], and the converse will be true under pure dimming [$\Delta(P - E) < 0$], as borne out in Table 4.

Surface dimming, both with and without atmospheric heating, strongly suppresses evaporation by depleting the radiative energy required to drive it ($\Delta E < 0$; Table 4), but the reduction in evaporation per unit dimming is substantially smaller under pure absorption than under pure dimming (i.e., per unit dimming $\Delta E_{PD} < \Delta E_{PA} < 0$, where subscripts PA and PD refer to the pure absorption and pure dimming cases, respectively). However, we know that moisture convergence increases under pure absorption ($\Delta E_{PA} < \Delta P_{PA} < 0$) and decreases under pure dimming ($\Delta P_{PD} < \Delta E_{PD} < 0$). Thus, the reduction in precipitation due to pure absorption must be smaller per unit dimming than that due to pure dimming ($\Delta P_{PD} < \Delta E_{PD} < \Delta E_{PA} < \Delta P_{PA} < 0$).

It is interesting to note that precipitation reduction per unit dimming in the realistic aerosol case is comparable to that of the pure dimming case (Table 4). As noted in section 2, the realistic aerosol case can be thought of as a combination of the pure dimming and pure absorption cases, plus aerosol microphysical effects. Aerosols may suppress precipitation via microphysical indirect effects in the model by reducing cloud droplet size, although this process only operates in stratiform and shallow cumulus clouds in GFDL AM3's formulation (Donner et al. 2011). The precipitation reduction in the pure dimming case (Table 4) is entirely driven by reduced convective precipitation and, in fact, slightly compensated for by a <10% increase in stratiform precipitation (not shown). In the realistic aerosol case, meanwhile, approximately 30% comes from reduced stratiform precipitation, suggesting that microphysical effects play a role in the precipitation reduction. It is reasonable, therefore, that the magnitude of precipitation suppression under realistic aerosol should resemble that of pure dimming, with the additional suppression from microphysical effects counteracting the reduced suppression from the absorption-driven

[2] This can be confirmed to the first order by comparing column-integrated changes in ω, which range from 21% to 37% across the idealized forcing simulations (see section 3c), to column-integrated changes in horizontal winds (zonal u and meridional v), which are <1% (0.3% for pure absorption, 0.5% for pure dimming, and <0.001% for pure heating; not shown).

component of the realistic dimming. However, direct comparison is limited by the factors discussed in section 2. These microphysical effects may also explain some of the difference in subregional meridional structure between ω_{500} and precipitation in the realistic aerosol case (Fig. 4a vs Fig. 5a).

The above explanation reveals that, under the moisture convergence constraints imposed by their relative top-of-the-atmosphere radiative forcing, the relationship between the precipitation reduction with and without atmospheric heating (or, equivalently, under purely absorption-driven dimming and that under purely scattering-driven dimming) is strongly influenced by their relative reductions in surface evaporation. Fully understanding why dimming with atmospheric heating produces a smaller precipitation reduction per unit dimming than dimming without, therefore, requires an understanding of why combined surface dimming and atmospheric heating produce a smaller evaporation reduction per unit dimming. In the next section, we explore the physical mechanisms behind this difference in the surface energy balance response to pure dimming and pure absorption.

b. *Absorption's impact on surface energy flux response partitioning*

Aerosol-driven surface dimming over much of South and East Asia is thought to be compensated for largely by a reduction in latent heat release or evaporation (Ramanathan et al. 2001, 2005), consistent with our realistic aerosol case. In fully ocean–atmosphere coupled GCM runs conducted by Ramanathan et al. (2005), the evaporation decrease is strongly controlled on a regional basis by a reduction of the temperature and humidity gradient between the surface and boundary layer due to dimming-driven surface cooling. This surface latent heat flux reduction can further exacerbate transport-driven moisture deficits due to aerosols, such as those discussed in section 3c.

Our idealized perturbation results, however, indicate that whether decreased surface latent or sensible heat flux provides the larger balance for reduced shortwave radiation depends on the degree to which that dimming is concurrent with atmospheric heating (Table 2); in the absence of atmospheric heating, dimming is compensated for most strongly by a latent heat flux reduction, but in the presence of heating it is compensated for most strongly by a sensible heat flux reduction (section 3b). As discussed in section 4a, this outcome helps to explain the smaller precipitation reduction under pure absorption than under pure dimming. To understand the relative magnitude of the latent heat flux reduction, we first analyze the factors controlling the behavior of the complementary sensible heat flux reduction.

Sensible heat flux can be thought of as controlled by the local gradient between surface and near-surface atmospheric temperature and the wind speed. The change in horizontal wind speed over land is small under all four of our perturbations (shown at 850 mb in Fig. 3), less than 5% of climatological values at the near surface (10 m), so we focus here on the influence of the change in the gradient between surface and near-surface air temperature $\Delta T_s - \Delta T_a$ with (pure absorption) and without (pure dimming) atmospheric heating. Climatologically, the land surface is warmer than the near-surface atmosphere, encouraging the dry convection of turbulent heat flux from the surface to the atmosphere. If this gradient is depressed, by either land-surface cooling or atmospheric warming, the surface sensible heat flux will be proportionally depressed.

Pure absorption can be thought of as a superposition of pure dimming and pure heating, both of which exhibit a reduction in surface-to-air temperature gradient. In pure dimming, the depletion of surface shortwave radiation cools both the surface and the near-surface atmosphere (Fig. 6c), but more the surface than the atmosphere (Table 3), reducing the temperature gradient and suppressing surface sensible heat flux (Table 2). In pure heating, conversely, both surface and atmosphere warm (Fig. 6c and Table 3) as a result of the absorption-mimicking imposed shortwave heating. However, the atmosphere warms by more than the surface, again reducing the temperature gradient and, consequently, reducing surface sensible heat flux (Table 2) even in the absence of an imposed surface shortwave perturbation. In the pure absorption case, both the surface cooling from surface shortwave depletion and the atmospheric heating from in situ shortwave absorption are in operation. The combined effects result in a larger reduction in surface-to-air temperature gradient per unit dimming than under the pure dimming case [3.4 and 2.7 mK $(\mathrm{W\,m^{-2}})^{-1}$, respectively; Tables 3 and 1] and, consequently, stronger suppression of sensible heat flux per unit dimming [0.38 and 0.29 $\mathrm{W\,m^{-2}}$ $(\mathrm{W\,m^{-2}})^{-1}$, respectively; Table 2 and section 3b]. Thus, surface latent heat flux need not decrease as much for a given reduction in surface shortwave input as it does under the pure dimming conditions. As a result, latent heat flux (i.e., evaporation) suppression is weaker under pure absorption than under pure dimming, which (in combination with their relative influence on moisture convergence) helps explain the smaller precipitation reduction in the presence of atmospheric heating (section 4a).

We can also use the relative changes in near-surface atmospheric temperature between pure absorption and pure dimming to understand the relative reduction in

latent heat flux directly, although it is subject to more approximating assumptions. Climatologically, for a given net surface radiation, surface latent heat flux is controlled by the relative moisture content of the two reservoirs it communicates between: the land surface and the atmosphere. Over saturated surfaces (e.g., water or moist land), the surface latent heat flux is primarily determined by the near-surface atmospheric water demand, generally quantified as the potential evapotranspiration (PET) (e.g., Allen et al. 1998). Conversely, where near-surface atmospheric water demand is greater than surface water availability (e.g., arid land), variability in soil moisture is the primary controller of latent heat flux from the surface to the atmosphere (e.g., Seneviratne et al. 2010). Because of the climatologically high precipitation rates of the EASM, East Asian summertime latent heat flux is generally considered to be controlled by atmospheric water demand (e.g., Zhang et al. 2011). Thus, assuming that any changes in precipitation due to the imposed perturbations will not be sufficient to change the region from an atmosphere-controlled to a surface-controlled regime, the relative latent heat flux response to absorption-driven versus scattering-driven dimming can be understood by analyzing the relative impact of each on PET.

PET can be shown to be a direct function of surface air temperature T_a, subject to various simplifying assumptions (see Scheff and Frierson 2014). The smaller decrease in T_a under pure absorption than under pure dimming—a result of the balance between the atmospheric absorption-induced heating and surface dimming-induced cooling—leads to a smaller decrease in PET. Consequently, the near-surface atmosphere's demand for moisture, which will be the primary driver of latent heat flux under monsoon-saturated surface conditions, decreases by less per unit dimming under pure absorption than under pure dimming. Given the same amount of dimming, therefore, the surface shortwave flux reduction will have to be more strongly balanced by reduced sensible heat flux under pure absorption (section 3b), as the latent heat flux reduction will be limited by the atmosphere's relatively greater demand for moisture under pure absorption than under pure dimming.

c. *Atmospheric processing of absorption-driven atmospheric heating*

The analysis in sections 4a and 4b demonstrates the competing interplay of absorbing aerosols differing surface, atmospheric, and top-of-the-atmosphere radiative perturbations. It is particularly important to note that the sign of local surface temperature change does not correspond to the sign of local TOA forcing in the case of aerosol absorption (Tables 1 and 3). By depleting surface shortwave radiation locally, absorbing aerosols can reduce regional surface temperatures, especially in regions in which the radiative–convective coupling of the surface and atmosphere is weak (Shindell and Faluvegi 2009; Ramanathan and Carmichael 2008; Bond et al. 2013). They may, however, increase surface temperature elsewhere through tropospheric transport of their atmospheric heating (Menon et al. 2002; Teng et al. 2012). Although surface–atmosphere coupling is thought to be relatively strong during the EASM (Zhang et al. 2011), our results suggest that it is not sufficient to overcome the cooling effects of the surface dimming.

If the atmospheric heating from absorption does not efficiently heat the surface, where does it go? Analysis of the perturbations to various components of the atmospheric heating rates sheds light on this question (Fig. 7). In the case of pure heating (Fig. 7b), negative dynamical heating primarily compensates for the imposed shortwave atmospheric heating, indicating that the heat is being transported out of the region. The dynamical heating perturbation peaks near 400 mb, indicating ventilation primarily in the upper atmosphere. This completes the circulation pattern indicated by the onshore flow at 850 mb and ascending motion through 500 mb (section 3c). There is weak cooling in the lower troposphere from vertical diffusion—a signal of the vertical propagation of the surface sensible heat flux suppression discussed in section 4b.

Under pure absorption (Fig. 7c), the clear-sky shortwave heating rate is similar by design to that in the pure heating simulation but is compensated for differently. There is some balancing by dynamical cooling aloft, suggesting a similar upper-atmospheric ventilation as in the pure heating case. However, there is a larger lower-atmospheric compensation by cooling from vertical diffusion than in the pure heating case. This can again be attributed to vertical propagation of pure absorption's large sensible heat flux suppression. Pure dimming exhibits lower-tropospheric cooling from vertical diffusion, which balances lower-tropospheric dynamical heating from the suppression of vertical motion described in section 4a and is consistent with the dimming-driven suppression of sensible heat flux discussed in section 4b. However, pure absorption's vertical diffusional cooling is a superposition of that both from pure heating atmosphere-driven sensible heat flux suppression and from the dimming-driven sensible heat flux suppression in the pure dimming case and therefore is substantially stronger, as with the surface sensible heat flux suppression itself.

The heating rate responses to aerosol absorption's shortwave heating demonstrate how a local positive aerosol radiative forcing can coexist with negative

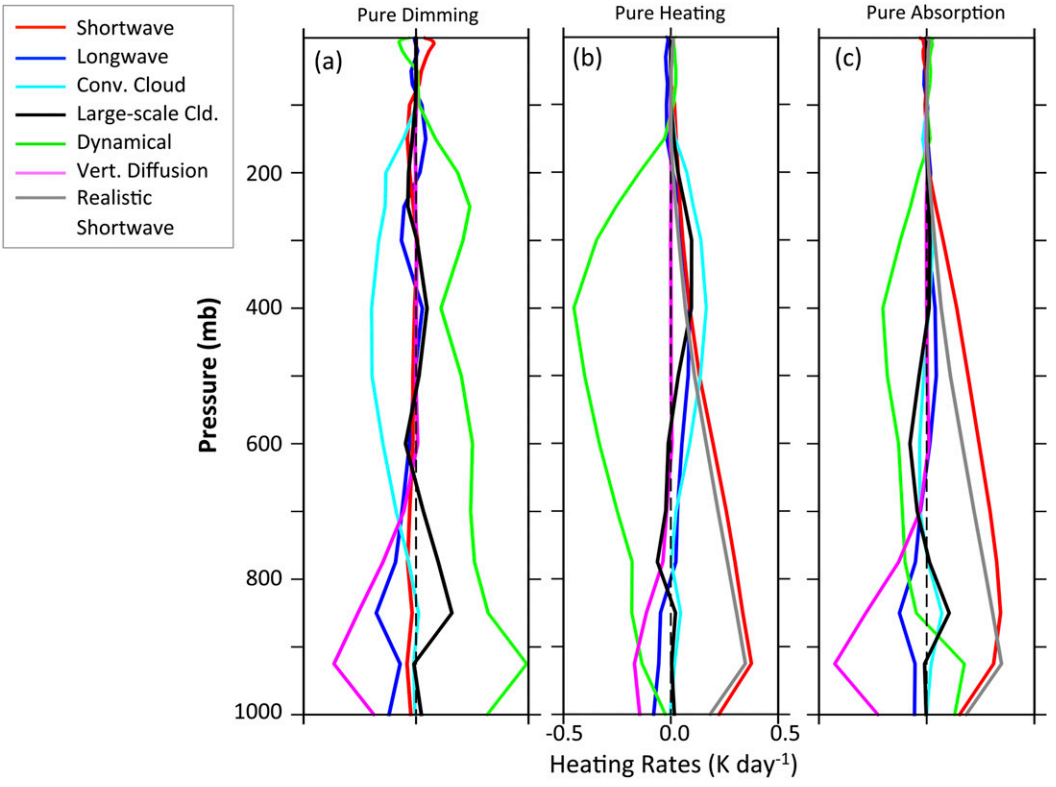

FIG. 7. Regional-mean atmospheric heating rates (K day^{-1}) are shown for the three idealized forcing simulations: (a) pure dimming, (b) pure heating, and (c) pure absorption. The heating rates due to shortwave (red) and longwave (dark blue) radiation, latent heat release by convective (light blue) and large-scale (black) cloud formation, vertical diffusion (pink), and dynamical advection of sensible heat (green; computed as residual of other terms) are shown. The shortwave heating rate for the realistic aerosol case is also shown (gray) for reference in (b) and (c).

regional surface responses through transport of the heating out of the forcing region. Given the inherently regional nature of aerosol forcing, because of aerosols' short lifetime and geographically concentrated emissions sources, this result demonstrates that local responses to changes in absorbing aerosol emissions should not be expected to follow global-mean responses and that the surface heating effects from such changes in one region may be primarily felt in other regions.

d. Limitations of this work

It is important to note that our study, by fixing SSTs to observations, does not incorporate the potential additional EASM impacts of the ocean-mediated response to our regional perturbations. The total regional response to aerosols can be linearly decomposed into the fast land-and-atmosphere response and the slower ocean-coupled response (Hsieh et al. 2013). It is valuable, therefore, to understand each part in isolation—for example, in order to understand the time evolution of the observed response following a rapid decline in regional aerosol emissions. The radiative forcing that the perturbations analyzed here impose in the global mean is orders of magnitude smaller than what they impose at the regional level. Consequently, we would expect regional-scale SST-mediated changes in the hydrological cycle to be more important than global-mean SST-mediated changes (e.g., Ming et al. 2010; Samset et al. 2016) under ocean-coupled conditions.

Our imposed regional perturbations could modify adjacent SSTs and thus induce local ocean-mediated effects on East Asian precipitation and circulation. Because our idealized forcing perturbations are concentrated solely over land, they would only affect adjacent SSTs indirectly—for example, through circulation-induced changes in ocean surface fluxes. In the case of realistic aerosols, emissions from land-based sources can be transported over the ocean (e.g., Yu et al. 2008; Wang et al. 2014; Dallafior et al. 2015) where they can decrease Pacific SSTs by reducing surface shortwave radiation (e.g., Boo et al. 2015; Dallafior et al. 2016), which might relax the land–sea contrast induced by regional aerosols under our fixed SST conditions. We expect these ocean-mediated effects to be secondary to the large direct

effect that the in situ forcing has on the land surface (e.g., Hsieh et al. 2013), but their study could constitute an interesting extension of this work.

The complexity of the competing effects of aerosols' surface and atmospheric effects on EASM strength seen in the GFDL AM3 model in our idealized forcing framework highlights the importance of conducting such simulations in other model suites. The East Asian region of interest in this work is one over which CMIP5 models show agreement on the sign of precipitation response to absorbing aerosols, suggesting that the basic dynamics of the EASM response to absorbing aerosols is robust across models (Richardson et al. 2016). However, there are several relevant absorbing aerosol properties that remain a source of divergence in models (Bond et al. 2013): models disagree on the simulated vertical profile of absorbing aerosols, and the efficiency with which black carbon absorbs shortwave radiation remains uncertain, tied particularly to variability in how models parameterize mixing of different aerosol species—deficiencies that stem partly from the limited nature of vertically resolved observations of aerosol properties. The realistic aerosol atmospheric distributions produced by GFDL AM3 [i.e., those from which the vertical profiles of aerosol optical depth (AOD) and heating rate in the idealized forcing experiments are derived] have been compared with available observations in Ocko and Ginoux (2017). Comparison over East Asia suggests that GFDL AM3's aerosol extinction coefficients in JJA are larger and more vertically diffuse than those seen in observations, although in both cases AOD remains strongly concentrated below 2 km. We expect the physical arguments laid out in this study, however, to be robust to vertical distributions within the current uncertainty range, as they are based either on vertically integrated frameworks (section 4a) or on secular changes that we expect to hold in the presence of any bottom-weighted atmospheric heating (sections 4b and 4c).

To our knowledge, no other modeling study has separated the surface and atmospheric effects of aerosol absorption over East Asia. The highly idealized nature of our forcings also precludes direct comparison with observations other than that discussed in section 2. Some other studies, however, have separately simulated the effects of BC aerosol on the EASM. Such analysis can be most closely compared with the results of our pure absorption simulation (although it should be noted that the pure absorption simulation, as a radiative idealization, is not a direct analog for the effects of BC emissions, which would be influenced by interactive transport and internal mixing with sulfate). Huang et al. (2007) and Wang et al. (2015) isolate the direct effects of BC in two generations of the RegCCM regional climate model over East Asia. Both studies find that summer precipitation decreases in the presence of BC. These studies also simulate the EASM response to all anthropogenic aerosols, and comparison of the ratio of precipitation reduction to surface dimming in their BC-only versus all-aerosol simulations corroborates our finding that absorption-driven dimming reduces precipitation by less than scattering-driven dimming. However, the driving mechanisms behind this result are not analyzed in those studies and thus cannot be compared with those discussed here. At the same time, Guo et al. (2013) find no effect of BC on June–July precipitation in East Asia (although August–September precipitation reductions do occur in response to BC) in a high-resolution model, and Folini and Wild (2015) find that modeled BC emissions trends do not contribute significantly to summertime precipitation trends in East Asia from 1990 to 2005. The diversity of precipitation responses to BC seen in model studies highlights the necessity of understanding the mechanisms underlying absorbing aerosols' impact on the EASM and the value of idealized studies such as this.

5. Conclusions

The impact of absorbing aerosols on regional climate manifests through their impact both on the atmospheric radiative budget and on surface energy fluxes. This work provides one of the first analyses of the separate and combined effects of aerosol absorption's atmospheric and surface perturbations on East Asian summertime climate. Our work suggests that the surface energy impacts of aerosol absorption are capable of outweighing its atmospheric impacts in the net response of East Asian summer monsoon (EASM) strength, resulting in a net decrease of EASM circulation and precipitation due to the reduced land–sea contrast from dimming-induced land-surface cooling (section 3c). Crucially, however, the precipitation reduction is smaller per unit dimming when that dimming is combined with the atmospheric heating from absorbing aerosols than when it acts in isolation, because of the moisture convergence constraints imposed by the positive top-of-the-atmosphere radiative forcing associated with absorbing aerosols (section 4a). This is partially influenced by stronger suppression of surface sensible heat than latent heat in the presence of the atmospheric effects of absorption and converse behavior in their absence (section 4b), which constrains the relative reduction in the evaporative component of moisture convergence and consequently the relative reduction in the precipitation component. Atmospheric heating from aerosol

absorption plays a role in this additional suppression of sensible heat, but it is primarily transported out of the region in the upper troposphere (section 4c). Consequently, absorbing aerosols' impact on East Asian summertime climate more closely resembles the response to its surface dimming than to its atmospheric heating. These contrasts between the effects of absorbing aerosols with and without their atmospheric heating can also be interpreted as contrasts between the effects of surface dimming from absorbing versus scattering aerosols.

The partitioning of the surface energy balance between sensible and latent heat flux (i.e., the Bowen ratio SH/LH) has myriad implications for surface temperature, convection, and boundary layer depth, as well as the atmospheric moisture budget (e.g., Andrews et al. 2009). Our results indicate that this partitioning is sensitive to the atmospheric forcing associated with a surface forcing: dimming with and without atmospheric heating perturb the Bowen ratio in opposite directions. We provide a physical explanation here for why sensible heat suppression dominates latent heat suppression under purely absorption-driven dimming, but the partitioning of surface energy fluxes is known to be underconstrained in climate models (e.g., Dirmeyer 2011). The impact that this partitioning can have on the magnitude of a precipitation response to solar dimming (section 4a) highlights the importance of better constraining this process in models.

This analysis sheds light on the response of East Asian summertime climate to realistic regional aerosol emissions. Surface solar radiation reductions over this region since the 1960s have been driven equally by increased aerosol scattering and increased aerosol absorption (Persad et al. 2014). However, the negative EASM response to historical regional aerosol emissions (realistic aerosol)—a net reduction of onshore flow, atmospheric ascent, and regional-mean precipitation—scales in proportion to purely scattering-driven dimming (pure dimming; section 4a) and does not exhibit the signal of absorption-driven atmospheric heating (pure heating), which on its own invigorates EASM circulation (section 3c). That even purely absorption-driven dimming reduces EASM strength helps explain why the combined absorption- and scattering-driven dimming of realistic aerosols shows such a strong EASM reduction. Additionally, our analysis of heating rates (section 4c) highlights the ways in which atmospheric heating from absorbing aerosols may be transported out of the region rather than warming the surface locally.

Our idealized forcing simulations, in addition to providing physical insight on the interaction of absorbing aerosols with the EASM, provide test cases at the two limits of possible future absorption-to-scattering ratios of East Asian aerosol emissions. Since 2000, scattering sulfate emissions have plateaued and declined (Klimont et al. 2013; Li et al. 2013), while absorbing black carbon emissions have continued to rise (Lei et al. 2011) and are expected to continue to do so at least through 2030 (e.g., Levy 2009). The pure absorption simulation provides an extreme test case of a situation in which East Asia's aerosol concentrations are dominated by absorbing rather than scattering aerosols—for example, if China continues to mitigate sulfate aerosol emissions without imposing significant controls on black carbon aerosol emissions. Conversely, the pure dimming case provides an extreme test of a scenario in which China mitigates its absorbing black carbon emissions without mitigating its scattering sulfate emissions. In combination, these two simulations suggest that increases in either aerosol type will have detrimental effects on EASM strength, but that BC-driven dimming may be less detrimental than sulfate-driven dimming.

Acknowledgments. The authors thank Paul Ginoux for feedback on the early stages of this research and Tom Delworth and Isaac Held for helpful comments on the initial manuscript. G. G. Persad was partly supported during this work by the National Science Foundation Graduate Research Fellowship under Grant DGE-1148900.

REFERENCES

Albrecht, B. A., 1989: Aerosols, cloud microphysics, and fractional cloudiness. *Science*, **245**, 1227–1230, doi:10.1126/science.245.4923.1227.

Allen, R. J., L. S. Pereira, D. Raes, and M. Smith, 1998: Crop evapotranspiration: Guidelines for computing crop water requirements. FAO Irrigation and Drainage Paper 56, 15 pp., https://appgeodb.nancy.inra.fr/biljou/pdf/Allen_FAO1998.pdf.

——, J. R. Norris, and M. Wild, 2013: Evaluation of multidecadal variability in CMIP5 surface solar radiation and inferred underestimation of aerosol direct effects over Europe, China, Japan, and India. *J. Geophys. Res. Atmos.*, **118**, 6311–6336, doi:10.1002/jgrd.50426.

Andrews, T., P. M. Forster, and J. M. Gregory, 2009: A surface energy perspective on climate change. *J. Climate*, **22**, 2557–2570, doi:10.1175/2008JCLI2759.1.

Bollasina, M. A., Y. Ming, and V. Ramaswamy, 2011: Anthropogenic aerosols and the weakening of the South Asian summer monsoon. *Science*, **334**, 502–505, doi:10.1126/science.1204994.

Bond, T. C., and Coauthors, 2013: Bounding the role of black carbon in the climate system: A scientific assessment. *J. Geophys. Res. Atmos.*, **118**, 5380–5552, doi:10.1002/jgrd.50171.

Boo, K.-O., B. B. B. Booth, Y.-H. Byun, J. Lee, C. Cho, S. Shim, and K.-T. Kim, 2015: Influence of aerosols in multidecadal SST variability simulations over the North Pacific. *J. Geophys. Res. Atmos.*, **120**, 517–531, doi:10.1002/2014JD021933.

Chen, J., and S. Bordoni, 2014: Orographic effects of the Tibetan Plateau on the East Asian summer monsoon: An energetic perspective. *J. Climate*, **27**, 3052–3072, doi:10.1175/JCLI-D-13-00479.1.

Chou, C., and J. D. Neelin, 2003: Mechanisms limiting the northward extent of the northern summer monsoons over North America, Asia, and Africa. *J. Climate*, **16**, 406–425, doi:10.1175/1520-0442(2003)016<0406:MLTNEO>2.0.CO;2.

Chung, C. E., V. Ramanathan, and J. T. Kiehl, 2002: Effects of the South Asian absorbing haze on the northeast monsoon and surface-air heat exchange. *J. Climate*, **15**, 2462–2476, doi:10.1175/1520-0442(2002)015<2462:EOTSAA>2.0.CO;2.

Dai, A., H. Li, Y. Sun, L.-C. Hong, L. Ho, C. Chou, and T. Zhou, 2013: The relative roles of upper and lower tropospheric thermal contrasts and tropical influences in driving Asian summer monsoons. *J. Geophys. Res. Atmos.*, **118**, 7024–7045, doi:10.1002/jgrd.50565.

Dallafior, T. N., D. Folini, R. Knutti, and M. Wild, 2015: Dimming over the oceans: Transient anthropogenic aerosol plumes in the twentieth century. *J. Geophys. Res. Atmos.*, **120**, 2014JD022 658, doi:10.1002/2014JD022658.

——, ——, ——, and ——, 2016: Mixed-layer ocean responses to anthropogenic aerosol dimming from 1870 to 2000. *J. Geophys. Res. Atmos.*, **121**, 3465–3484, doi:10.1002/2014JD022658.

Dirmeyer, P. A., 2011: A history and review of the Global Soil Wetness Project (GSWP). *J. Hydrometeor.*, **12**, 729–749, doi:10.1175/JHM-D-10-05010.1.

Donner, L. J., and Coauthors, 2011: The dynamical core, physical parameterizations, and basic simulation characteristics of the atmospheric component AM3 of the GFDL global coupled model CM3. *J. Climate*, **24**, 3484–3519, doi:10.1175/2011JCLI3955.1.

Dwyer, J. G., J. R. Norris, and C. Ruckstuhl, 2010: Do climate models reproduce observed solar dimming and brightening over China and Japan? *J. Geophys. Res.*, **115**, D00K08, doi:10.1029/2009JD012945.

Erlick, C., V. Ramaswamy, and L. M. Russell, 2006: Differing regional responses to a perturbation in solar cloud absorption in the SKYHI general circulation model. *J. Geophys. Res.*, **111**, D06204, doi:10.1029/2005JD006491.

Feingold, G., 2005: On smoke suppression of clouds in Amazonia. *Geophys. Res. Lett.*, **32**, L02804, doi:10.1029/2004GL021369.

Folini, D., and M. Wild, 2015: The effect of aerosols and sea surface temperature on China's climate in the late twentieth century from ensembles of global climate simulations. *J. Geophys. Res. Atmos.*, **120**, 2261–2279, doi:10.1002/2014JD022851.

Guo, L., E. J. Highwood, L. C. Shaffrey, and A. G. Turner, 2013: The effect of regional changes in anthropogenic aerosols on rainfall of the East Asian summer monsoon. *Atmos. Chem. Phys.*, **13**, 1521–1534, doi:10.5194/acp-13-1521-2013.

Guo, Z., T. Zhou, M. Wang, and Y. Qian, 2015: Impact of cloud radiative heating on East Asian summer monsoon circulation. *Environ. Res. Lett.*, **10**, 074014, doi:10.1088/1748-9326/10/7/074014.

Hansen, J. E., M. Sato, and R. Ruedy, 1997: Radiative forcing and climate response. *J. Geophys. Res.*, **102**, 6831–6864, doi:10.1029/96JD03436.

Hsieh, W.-C., W. D. Collins, Y. Liu, J. C. H. Chiang, C.-L. Shie, K. Caldeira, and L. Cao, 2013: Climate response due to carbonaceous aerosols and aerosol-induced SST effects in NCAR community atmospheric model CAM3.5. *Atmos. Chem. Phys.*, **13**, 7489–7510, doi:10.5194/acp-13-7489-2013.

Huang, Y., W. L. Chameides, and R. E. Dickinson, 2007: Direct and indirect effects of anthropogenic aerosols on regional precipitation over East Asia. *J. Geophys. Res.*, **112**, D03212, doi:10.1029/2006JD007114.

Jiang, Y., X. Liu, X.-Q. Yang, and M. Wang, 2013: A numerical study of the effect of different aerosol types on East Asian summer clouds and precipitation. *Atmos. Environ.*, **70**, 51–63, doi:10.1016/j.atmosenv.2012.12.039.

Johnson, B., K. Shine, and P. Forster, 2004: The semi-direct aerosol effect: Impact of absorbing aerosols on marine stratocumulus. *Quart. J. Roy. Meteor. Soc.*, **130**, 1407–1422, doi:10.1256/qj.03.61.

Kim, M. J., S.-W. Yeh, and R. J. Park, 2016: Effects of sulfate aerosol forcing on East Asian summer monsoon for 1985–2010. *Geophys. Res. Lett.*, **43**, 1364–1372, doi:10.1002/2015GL067124.

Klimont, Z., S. J. Smith, and J. Cofala, 2013: The last decade of global anthropogenic sulfur dioxide: 2000–2011 emissions. *Environ. Res. Lett.*, **8**, 014003, doi:10.1088/1748-9326/8/1/014003.

Koch, D., and A. D. Del Genio, 2010: Black carbon semi-direct effects on cloud cover: Review and synthesis. *Atmos. Chem. Phys.*, **10**, 7685–7696, doi:10.5194/acp-10-7685-2010.

Lamarque, J.-F., and Coauthors, 2010: Historical (1850–2000) gridded anthropogenic and biomass burning emissions of reactive gases and aerosols: Methodology and application. *Atmos. Chem. Phys.*, **10**, 7017–7039, doi:10.5194/acp-10-7017-2010.

Lei, Y., Q. Zhang, K. B. He, and D. G. Streets, 2011: Primary anthropogenic aerosol emission trends for China, 1990–2005. *Atmos. Chem. Phys.*, **11**, 931–954, doi:10.5194/acp-11-931-2011.

Levy, H., 2009: Climate projections based on emissions scenarios for long-lived and short-lived radiatively active gases and aerosols. U.S. Climate Change Science Program Rep., 116 pp.

Li, H., A. Dai, T. Zhou, and J. Lu, 2010: Responses of East Asian summer monsoon to historical SST and atmospheric forcing during 1950–2000. *Climate Dyn.*, **34**, 501–514, doi:10.1007/s00382-008-0482-7.

Li, J., and Q. Zeng, 2002: A unified monsoon index. *Geophys. Res. Lett.*, **29**, 1274, doi:10.1029/2001GL013874.

——, Z. Han, and Z. Xie, 2013: Model analysis of long-term trends of aerosol concentrations and direct radiative forcings over East Asia. *Tellus*, **65B**, 20410, doi:10.3402/tellusb.v65i0.20410.

Li, X., M. Ting, C. Li, and N. Henderson, 2015: Mechanisms of Asian summer monsoon changes in response to anthropogenic forcing in CMIP5 models. *J. Climate*, **28**, 4107–4125, doi:10.1175/JCLI-D-14-00559.1.

Lu, R., B. Dong, and H. Ding, 2006: Impact of the Atlantic multidecadal oscillation on the Asian summer monsoon. *Geophys. Res. Lett.*, **33**, L24701, doi:10.1029/2006GL027655.

Ma, S., and Coauthors, 2017: Detectable anthropogenic shift toward heavy precipitation over eastern China. *J. Climate*, **30**, 1381–1396, doi:10.1175/JCLI-D-16-0311.1.

Meehl, G. A., J. M. Arblaster, and W. D. Collins, 2008: Effects of black carbon aerosols on the Indian monsoon. *J. Climate*, **21**, 2869–2882, doi:10.1175/2007JCLI1777.1.

Menon, S., J. Hansen, L. Nazarenko, and Y. Luo, 2002: Climate effects of black carbon aerosols in China and India. *Science*, **297**, 2250–2253, doi:10.1126/science.1075159.

Ming, Y., V. Ramaswamy, L. J. Donner, and V. T. Phillips, 2006: A new parameterization of cloud droplet activation applicable to general circulation models. *J. Atmos. Sci.*, **63**, 1348–1356, doi:10.1175/JAS3686.1.

——, ——, ——, ——, S. A. Klein, P. A. Ginoux, and L. W. Horowitz, 2007: Modeling the interactions between aerosols and liquid water clouds with a self-consistent cloud scheme in a general circulation model. *J. Atmos. Sci.*, **64**, 1189–1209, doi:10.1175/JAS3874.1.

——, ——, and G. Persad, 2010: Two opposing effects of absorbing aerosols on global-mean precipitation. *Geophys. Res. Lett.*, **37**, L13701, doi:10.1029/2010GL042895.

Myhre, G., and Coauthors, 2013: Anthropogenic and natural radiative forcing. *Climate Change 2013: The Physical Science Basis*, T. F. Stocker et al., Eds., Cambridge University Press, 659–740.

Neelin, J. D., and I. M. Held, 1987: Modeling tropical convergence based on the moist static energy budget. *Mon. Wea. Rev.*, **115**, 3–12, doi:10.1175/1520-0493(1987)115<0003:MTCBOT>2.0.CO;2.

Norris, J. R., and M. Wild, 2009: Trends in aerosol radiative effects over China and Japan inferred from observed cloud cover, solar ''dimming,'' and solar ''brightening.'' *J. Geophys. Res.*, **114**, D00D15, doi:10.1029/2008JD011378.

Ocko, I. B., and P. A. Ginoux, 2017: Comparing multiple model-derived aerosol optical properties to spatially collocated ground-based and satellite measurements. *Atmos. Chem. Phys.*, **17**, 4451–4475, doi:10.5194/acp-17-4451-2017.

——, V. Ramaswamy, P. Ginoux, Y. Ming, and L. W. Horowitz, 2012: Sensitivity of scattering and absorbing aerosol direct radiative forcing to physical climate factors. *J. Geophys. Res.*, **117**, D20203, doi:10.1029/2012JD018019.

Persad, G. G., Y. Ming, and V. Ramaswamy, 2012: Tropical tropospheric-only responses to absorbing aerosols. *J. Climate*, **25**, 2471–2480, doi:10.1175/JCLI-D-11-00122.1.

——, ——, and ——, 2014: The role of aerosol absorption in driving clear-sky solar dimming over East Asia. *J. Geophys. Res. Atmos.*, **119**, 10 410–10 424, doi:10.1002/2014JD021577.

Qian, Y., D. P. Kaiser, L. R. Leung, and M. Xu, 2006: More frequent cloud-free sky and less surface solar radiation in China from 1955 to 2000. *Geophys. Res. Lett.*, **33**, L01812, doi:10.1029/2005GL024586.

——, W. Wang, L. R. Leung, and D. P. Kaiser, 2007: Variability of solar radiation under cloud-free skies in China: The role of aerosols. *Geophys. Res. Lett.*, **34**, L12804, doi:10.1029/2006GL028800.

Ramanathan, V., and G. Carmichael, 2008: Global and regional climate changes due to black carbon. *Nat. Geosci.*, **1**, 221–227, doi:10.1038/ngeo156.

——, P. J. Crutzen, J. T. Kiehl, and D. Rosenfeld, 2001: Aerosols, climate, and the hydrological cycle. *Science*, **294**, 2119–2124, doi:10.1126/science.1064034.

——, and Coauthors, 2005: Atmospheric brown clouds: Impacts on South Asian climate and hydrological cycle. *Proc. Natl. Acad. Sci. USA*, **102**, 5326–5333, doi:10.1073/pnas.0500656102.

Randles, C. A., and V. Ramaswamy, 2008: Absorbing aerosols over Asia: A Geophysical Fluid Dynamics Laboratory general circulation model sensitivity study of model response to aerosol optical depth and aerosol absorption. *J. Geophys. Res.*, **113**, D21203, doi:10.1029/2008JD010140.

Rayner, N. A., D. E. Parker, E. B. Horton, C. K. Folland, L. V. Alexander, D. P. Rowell, E. C. Kent, and A. Kaplan, 2003: Global analyses of sea surface temperature, sea ice, and night marine air temperature since the late nineteenth century. *J. Geophys. Res.*, **108**, 4407, doi:10.1029/2002JD002670.

Richardson, T. B., P. M. Forster, T. Andrews, and D. J. Parker, 2016: Understanding the rapid precipitation response to CO_2 and aerosol forcing on a regional scale. *J. Climate*, **29**, 583–594, doi:10.1175/JCLI-D-15-0174.1.

Roeckner, E., L. Bengtsson, J. Feichter, J. Lelieveld, and H. Rodhe, 1999: Transient climate change simulations with a coupled atmosphere–ocean GCM including the tropospheric sulfur cycle. *J. Climate*, **12**, 3004–3032, doi:10.1175/1520-0442(1999)012<3004:TCCSWA>2.0.CO;2.

Salzmann, M., H. Weser, and R. Cherian, 2014: Robust response of Asian summer monsoon to anthropogenic aerosols in CMIP5 models. *J. Geophys. Res. Atmos.*, **119**, 11 321–11 337, doi:10.1002/2014JD021783.

Samset, B. H., and Coauthors, 2016: Fast and slow precipitation responses to individual climate forcers: A PDRMIP multi-model study. *Geophys. Res. Lett.*, **43**, 2782–2791, doi:10.1002/2016GL068064.

Santer, B. D., T. M. L. Wigley, J. S. Boyle, D. J. Gaffen, J. J. Hnilo, D. Nychka, D. E. Parker, and K. E. Taylor, 2000: Statistical significance of trends and trend differences in layer-average atmospheric temperature time series. *J. Geophys. Res.*, **105**, 7337–7356, doi:10.1029/1999JD901105.

Scheff, J., and D. M. W. Frierson, 2014: Scaling potential evapotranspiration with greenhouse warming. *J. Climate*, **27**, 1539–1558, doi:10.1175/JCLI-D-13-00233.1.

Seneviratne, S. I., T. Corti, E. L. Davin, M. Hirschi, E. B. Jaeger, I. Lehner, B. Orlowsky, and A. J. Teuling, 2010: Investigating soil moisture–climate interactions in a changing climate: A review. *Earth Sci. Rev.*, **99**, 125–161, doi:10.1016/j.earscirev.2010.02.004.

Shindell, D., and G. Faluvegi, 2009: Climate response to regional radiative forcing during the twentieth century. *Nat. Geosci.*, **2**, 294–300, doi:10.1038/ngeo473.

Song, F., and T. Zhou, 2014: The climatology and interannual variability of East Asian summer monsoon in CMIP5 coupled models: Does air–sea coupling improve the simulations? *J. Climate*, **27**, 8761–8777, doi:10.1175/JCLI-D-14-00396.1.

——, ——, and Y. Qian, 2014: Responses of East Asian summer monsoon to natural and anthropogenic forcings in the 17 latest CMIP5 models. *Geophys. Res. Lett.*, **41**, 596–603, doi:10.1002/2013GL058705.

Sperber, K. R., H. Annamalai, I.-S. Kang, A. Kitoh, A. Moise, A. Turner, B. Wang, and T. Zhou, 2013: The Asian summer monsoon: An intercomparison of CMIP5 vs. CMIP3 simulations of the late 20th century. *Climate Dyn.*, **41**, 2711–2744, doi:10.1007/s00382-012-1607-6.

Streets, D. G., and Coauthors, 2009: Anthropogenic and natural contributions to regional trends in aerosol optical depth, 1980–2006. *J. Geophys. Res.*, **114**, D00D18, doi:10.1029/2008JD011624.

——, D. T. Shindell, Z. Lu, and G. Faluvegi, 2013: Radiative forcing due to major aerosol emitting sectors in China and India. *Geophys. Res. Lett.*, **40**, 4409–4414, doi:10.1002/grl.50805.

Tao, S. Y., and L. X. Chen, 1987: A review of recent research on the East Asian summer monsoon in China. *Review of Monsoon Meteorology*, C. P. Chang and T. K. Krishnamurthy, Eds., Oxford University Press, 60–92.

Teng, H., W. M. Washington, G. Branstator, G. A. Meehl, and J.-F. Lamarque, 2012: Potential impacts of Asian carbon aerosols on future US warming. *Geophys. Res. Lett.*, **39**, L11703, doi:10.1029/2012GL051723.

Twomey, S., 1977: The influence of pollution on the shortwave albedo of clouds. *J. Atmos. Sci.*, **34**, 1149–1152, doi:10.1175/1520-0469(1977)034<1149:TIOPOT>2.0.CO;2.

Wang, B., Z. Wu, J. Li, J. Liu, C.-P. Chang, Y. Ding, and G. Wu, 2008: How to measure the strength of the East Asian

summer monsoon. *J. Climate*, **21**, 4449–4463, doi:10.1175/2008JCLI2183.1.

Wang, C., 2004: A modeling study on the climate impacts of black carbon aerosols. *J. Geophys. Res.*, **109**, D03106, doi:10.1029/2003JD004084.

Wang, T. J., and Coauthors, 2015: The interactions between anthropogenic aerosols and the East Asian summer monsoon using RegCCMS. *J. Geophys. Res. Atmos.*, **120**, 5602–5621, doi:10.1002/2014JD022877.

Wang, Y., and Coauthors, 2014: Assessing the effects of anthropogenic aerosols on Pacific storm track using a multiscale global climate model. *Proc. Natl. Acad. Sci. USA*, **111**, 6894–6899, doi:10.1073/pnas.1403364111.

Webster, P., 1987: The elementary monsoon. *Monsoons*, J. S. Fein and P. L. Stephens, Eds., John Wiley and Sons, 3–32.

Yu, H., L. A. Remer, M. Chin, H. Bian, R. G. Kleidman, and T. Diehl, 2008: A satellite-based assessment of transpacific transport of pollution aerosol. *J. Geophys. Res.*, **113**, D14S12, doi:10.1029/2007JD009349.

Zhang, J., L. Wu, and W. Dong, 2011: Land-atmosphere coupling and summer climate variability over East Asia. *J. Geophys. Res.*, **116**, D05117, doi:10.1029/2010JD014714.